Biomedical Signal Processing and Control 87 (2024) 105438

Contents lists available at ScienceDirect

Biomedical Signal Processing and Control

journal homepage: www.elsevier.com/locate/bspc

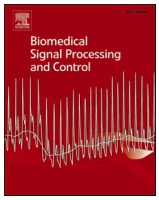

Using chemosensory-induced EEG signals to identify patients with *de novo* Parkinson's disease

B. Orkan Olcay [a,b,*], Fatih Onay [a,c], Güliz Akın Öztürk [d], Adile Öniz [e,g], Murat Özgören [e,f], Thomas Hummel [h], Çağdaş Güdücü [d]

[a] Department of Electrical and Electronics Engineering, Izmir Institute of Technology, 35430 Urla, Izmir, Turkey
[b] Institute of Health Sciences, Department of Neuroscience, Ege University, 35040 Bornova, Izmir, Turkey
[c] Department of Mechatronics Engineering, Faculty of Engineering and Natural Sciences, Bursa Technical University, 16310 Yıldırım, Bursa, Turkey
[d] Department of Biophysics, Faculty of Medicine, Dokuz Eylül University, 35410 Balçova, Izmir, Turkey
[e] Institute of Graduate Studies, Department of Neuroscience, Near East University, 99138 Nicosia, Cyprus
[f] Department of Biophysics, Faculty of Medicine, Near East University, 99138 Nicosia, Cyprus
[g] Faculty of Health Sciences, Near East University, 99138 Nicosia, Cyprus
[h] Smell & Taste Clinic, Department of Otorhinolaryngology, TU Dresden, 01307 Dresden, Germany

ARTICLE INFO

Keywords:
Parkinson's disease
Olfaction
Functional connectivity
Entropy
Feature extraction
Classification

ABSTRACT

Objective: Parkinson's disease (PD) patients generally exhibit an olfactory loss. Hence, psychophysical or electrophysiological tests are used for diagnosis. However, these tests are susceptible to the subjects' behavioral response bias and require advanced techniques for an accurate analysis.
Proposed Approach: Using well-known feature extraction methods, we characterized chemosensory-induced EEG responses of the participants to classify whether they have PD. The classification was performed for different time intervals after chemosensory stimulation to see which temporal segment better separates healthy controls and subjects with *de novo* PD.
Results: The performances show that entropy and connectivity features discriminate effectively PD and HC participants when olfactory-induced EEG signals were used. For these methods, discrimination is over 80% for segments 100–700 and 200–800 milliseconds after stimulus onset.
Comparison with Existing Methods: We compared the performance of our framework with linear predictive coding, bispectrum, wavelet entropy-based methods, and TDI score-based classification. While the entropy- and connectivity-based methods elicited the highest classification performances for olfactory stimuli, the linear predictive coding-based method elicited slightly higher performance than our framework when the trigeminal stimuli were used.
Conclusion: This is one of the first studies that use chemosensory-induced EEG signals along with different feature extraction methods to classify healthy subjects and subjects with *de novo* PD. Our results show that entropy and functional connectivity methods unravel the chemosensory-induced neural dynamics encapsulating critical information about the subjects' olfactory performance. Furthermore, time- and frequency-resolved feature analysis is beneficial for capturing disease-affected neural patterns.

1. Introduction

The neurological disorders can alter the brain dynamics significantly [1–5]. These alterations may stem from a variation in the information-processing machinery of the brain, which demonstrates itself as a change in inter-regional functional connectivity and changes in complex dynamics of oscillatory activity in many brain regions [5–9]. Detecting these alterations due to neurodegenerative diseases is crucial for early diagnosis, which may help to maintain the patients' quality of life via alternative treatments.

* Corresponding author at: Department of Electrical and Electronics Engineering, Izmir Institute of Technology, 35430 Urla, Izmir, Turkey.
E-mail addresses: bilalolcay@iyte.edu.tr, orkanolcay@gmail.com (B.O. Olcay), fatih.onay@btu.edu.tr, fatihonay@iyte.edu.tr (F. Onay), guliz.akinozturk@ogr.deu.edu.tr (G. Akın Öztürk), adile.oniz@neu.edu.tr (A. Öniz), murat.ozgoren@neu.edu.tr (M. Özgören), thomas.hummel@tu-dresden.de (T. Hummel), cagdas.guducu@deu.edu.tr (Ç. Güdücü).

https://doi.org/10.1016/j.bspc.2023.105438
Received 29 March 2023; Received in revised form 12 July 2023; Accepted 12 September 2023
Available online 19 September 2023

Parkinson's disease (PD) is the second most common neurological disease that affects more than 10 million people worldwide [10]. A vast number of brain networks are affected due to PD, which may demonstrate itself as motor and non-motor symptoms such as tremors, rigidity, postural instability, visual impairment, cognitive decline, dysphonia, depression, apathy, and impairments in swallowing and breathing [11–14]. These symptoms have been demonstrated to be due to nigrostriatal dopamine depletion and pathophysiological perturbations of the brain [15–18]. Besides these symptoms, olfactory abnormalities, one of the most critical non-motor symptoms of PD, appear as an early biomarker of PD [19,20]. In that context, psychophysical and electrophysiological tests are critical for accurately examining chemosensory system performance for detecting PD or other neurological problems [21–23].

Detecting chemosensory abnormalities enable early treatment strategies that slow the disease progression [24]. Several studies have been conducted to understand the complex mechanism of olfactory function [25] and its relation to neurodegenerative disorders [23,26–29]. The results of these studies exhibit the importance of development of a diagnostic tool for chemosensory perception evaluation, especially for the diagnosis of PD.

Psychophysical tests have been demonstrated not to be enough for detecting PD when they are used as a single test [30]. Contrary to this, electrophysiological measures help to observe the PD-related changes of sensorial processing dynamics in the brain response patterns which enable us to obtain more information about the progression of PD [31,32]. The classical electrophysiological method for the olfactory performance evaluation is calculating the averages of time-locked event-related potentials and analyzing the amplitude and latency of these averaged potentials in the post-stimulus time interval. These potentials reflect the neocortical processes of olfactory information, which may become invisible in the case of functional lesions and neuronal loss [33]. However, these potentials may not be visible in normosmic (i.e., healthy controls) subjects and could be visible even if the subjects suffer from PD [33–35]. In that context, analyzing the amplitude and latency of brain potentials may not provide enough information about olfactory sensation [36]. Even if these cortical potentials are absent, the olfactory function can be evaluated by analyzing these brain signals using advanced methods [37–40].

The trigeminal system, also known to be closely related to the olfactory system, is responsible for warmth, burning, stinging, and freshness sensations [29]. There are large conflicting outcomes about the trigeminal system responses of PD patients. Whilst some studies have shown that PD patients elicit electrophysiological brain responses with lower amplitudes and prolonged latencies in response to trigeminal stimulus compared to healthy subjects [41–43]; some of these studies show that the trigeminal sensation remains intact [29,44,45]. These conflicting results may point that the trigeminal sensitivity in PD patients has different characteristics from that of the patients with other non-PD-related olfactory loss and appeared the same in healthy controls.

In the last decade, the studies were generally conducted via analysis of electrophysiological signals collected during resting, cognitive, and motor task states from healthy and PD subjects [17,46,47]. The neuropathological findings of these studies do not always match with the pre-investigated spatio-temporal patterns of PD [48]. By now, very few studies have analyzed the chemosensory-induced EEG responses through signal processing methods to recognize the subjects with *de Novo* Parkinson's (newly diagnosed patients with Parkinson's disease and not receiving any L-dopa treatment) [40,49].

In the literature, various neural activity characterization methods have been mainly used for brain-computer interface (BCI) purposes [50–56]. The majority of the PD detection studies incorporate these characterization methods to detect the neural alterations [7,17,57,58]. By using these methods, extracting and using the chemosensory-induced neural features could be considered as valuable since the smell performance decline is one of the first earliest symptoms of PD [30,59].

In the present study, we aimed to investigate the performances of different feature extraction methods for detecting abnormal chemosensory-induced EEG patterns in *de novo* PD patients. We used entropy, time-domain features, filter-bank common spatial patterns (FBCSP), and linear mutual information due to their success in previous studies [40,55,56,60–63]. To the best of our knowledge, this study is one of the initial attempts that incorporates different feature extraction methods to evaluate PD-related neural patterns obtained from chemosensory-induced EEG signals.

This paper is organized as follows. In Section 2, we describe the datasets, the feature extraction methods, and the operational flow diagram steps of the classification framework. In Section 3, the classification performances, as well as the related biophysical outcomes, are presented. In Section 4, the results considering current biophysical findings are discussed. The final section concludes the paper.

2. Materials and methods

2.1. EEG dataset

Twenty newly diagnosed (*de Novo*) Parkinson's Disease (PD) patients (7 men, mean age: 53.92 ± 9.04 years) and 12 healthy age and gender-matched controls (HC) (7 men; mean age: 52.42 ± 7.69 years) were included in this study. This EEG dataset has recently been used in [64] and in [49]. Healthy participants did not have any neurological or psychiatric diagnosis according to a general examination at the neurology outpatient department. The local ethical committee of the Dokuz Eylul University approved this study. Before the EEG analysis, the olfactory function of the subjects of both groups was evaluated via Sniffin' Stick Test [65]. The mean threshold scores (T) were 2.6 (±1.9) for PD and 5.2 (±2.0) for healthy controls, and the mean discrimination scores (D) were 9.8 (±2.4) for PD and 11.2 (±2.4) for healthy controls. Also, the mean identification scores (I) were 8.3 (±3.2) for PD and 12.1 (±1.8) for healthy controls [49]. All the subjects were examined by the same ENT specialist before the olfactory testing to detect and exclude the subjects with any sinonasal pathologies. The control participants had no prior diagnosis of any neurological and/or psychiatric disorders. The informed consent was taken from subjects before they participate in the study.

The brain responses are recorded via the 64-channel electroencephalography (EEG) system (Neuroscan 4.3, Synamps, USA) in an electromagnetically and acoustically isolated room. Embedded Microcontroller Stimulation Unit (EMISU) [66], an air dilution olfactometer (Om2b, Burghardt, Germany), and additional equipment such as a video recording system were used to track the subject's condition and movements during recordings. The olfactometer, which provides a continuous airflow (approximately 8 L/min) with a relative humidity of around 80% and a fixed temperature (36 °C), was used to deliver the stimuli to the participant's nose. In this study, carbon dioxide (CO_2) and 2-phenyl–ethyl-alcohol (PEA) were used as specific trigeminal and olfactory stimulants, respectively [28,30]. The former stimulant is used to analyze the responses that mainly stem from the trigeminal system, and the latter is for analyzing responses that mainly arise from the olfactory system. The intensities of the stimuli were 60% (v/v percent) for PEA; 50–60% (v/v percent) for CO_2. The inter-stimulus interval (ISI) was determined between 15 and 17 s randomly.

The EEG caps of appropriate size (Quik Cap, Neuromedical Supplies, USA) were placed on the head of the participants according to the international 10–20 electrode positions system [67]. The two earlobes were linked ($\frac{A_1+A_2}{2}$) with Ag/AgCl electrodes for the references. The EEG signals were recorded at a sampling rate of $Fs = 1$ kHz, which means each epoch has 64 × 3001 signal samples. The independent electrodes were placed 1 cm away from the outer regions of both canthi to minimize the interference of eye movements. The impedance of the electrodes was kept at approximately $\leq 5k\Omega$ during the recordings which

was quite lower than the recommended impedance (below 50 k Ω) for the EEG amplifiers. On the average, we used 24.9 ± 5.1 trials for PEA and 26.2 ± 2.66 trials for CO_2 stimulations. Please note that due to the large-amplitude artifacts (i.e., exceeding 50 μV) observed in their most of the EEG epochs collected during CO_2 (trigeminal stimuli) presentation sessions (approximately 18.31 ± 3.49 trials were labeled as noisy), two HC and one PD subjects' EEG recordings were excluded from the further analyses. Thus, we had 32 and 29 subjects' EEG signals for PEA and CO_2 stimulation sessions, respectively.

The timings and the corresponding stimulus-induced EEG responses of each chemosensory stimulus were marked and registered by the EMISU (Embedded Interactive Stimulation Unit) [66].

2.2. EEG preprocessing

Before feature extraction, we first re-referenced the EEG signals via common average reference (CAR) to accentuate the region-specific neural patterns and attenuate the volume conduction and non-neural artifacts [68–70]. Then, the EEG channel signals were filtered using a high-pass filter with a cut-off frequency of 0.2 Hz to remove the low frequency voltage drifts. Thereafter, we filtered the EEG signals with a filter bank structure consisting of twelve 4^{th} order Butterworth filters to capture and use the frequency-resolved cortical activities, which is beneficial to elucidate the chemosensory stimulus-induced differences between subject groups [37]. Note that in this study, two-pass filtering (i.e., forward plus reverse filtering) was adopted to prevent the neural dynamics from phase shift due to filtering [57,71]. The frequency ranges of each filter in the bank structure are given in Table 1. These frequencies were selected according to previous neural activity characterization studies [55,72]. In those studies, the authors used nine frequency bands starting from four hertz, corresponding to the theta (θ) band. Here, we included three more filters into the bank structure to capture the chemosensory-related neural patterns embedded in lower and higher frequency bands since olfaction induces dynamic changes encoded in low as well as high-frequency bands [28,49,63,73,74].

After filtering, the epochs were extracted from the continuous EEG signals according to the chemosensory stimulus onset ($t = 0$). Each epoch started from 1000 milliseconds before the stimulus onset and lasted up to 2000 milliseconds after the stimulus onset. The timing diagram of an epoch were illustrated in Fig. 1.

2.3. Feature extraction methods

In this study, different feature extraction methods were used to characterize the EEG signals collected during chemosensory stimuli presentation. The details of the feature extraction are provided below. We evaluated the characterization performance of the features extracted from four different 600 ms-long time segments in the post-stimulus period as in [75]. The time windows that we used here: tw_1 comprises the temporal region $[100, 700]$ milliseconds starting from stimulus onset ($t = 0$), tw_2 the $[200, 800]$ milliseconds, tw_3 the $[300, 900]$ milliseconds, and tw_4 the $[400, 1000]$ milliseconds. We used these time windows to determine the time interval at which the brain provides the most distinctive features for PD versus HC subject classification. For the mathematical expression of each feature extraction method, we used the notation $s_{i,f}^{tw} = s_{i,f}(t)\big|_{t\in tw}$ which represents the signal segment obtained from the temporal region tw of channel i that was filtered in frequency band f. Throughout this study, we used the sampled version of the EEG signals $\tilde{s}_{i,f}^{tw}$. The mathematical expression of feature extraction methods is expressed by using the discrete signal expression $\tilde{s}_{i,f}^{tw}(n)$.

Table 1
The frequency bands of each 4th order Butterworth filter in the filter-bank structure. We presented the names and the respective frequency ranges of the twelve filters in the filter-bank structure here.

Filter Name	Frequency Band	Filter Name	Frequency Band
f_1	0–4 Hz	f_7	24–28 Hz
f_2	4–8 Hz	f_8	28–32 Hz
f_3	8–12 Hz	f_9	32–36 Hz
f_4	12–16 Hz	f_{10}	36–40 Hz
f_5	16–20 Hz	f_{11}	40–44 Hz
f_6	20–24 Hz	f_{12}	44–48 Hz

2.3.1. Entropy

We used the Kozachenko-Leonenko method for estimating the entropy, which was proposed in [76] and used in [40], to quantify the complexity of EEG signals. The entropy of the signal $\tilde{s}_{i,f}^{tw}(n)$ can be calculated using the formula.

$$M^{Entropy}\left(\tilde{s}_{i,f}^{tw}(n)\right) = -\psi(k) + \psi\left(N_{\tilde{s}_{i,f}^{tw}}\right) + \log c_d + \frac{d}{N_{\tilde{s}}}\sum_{p=1}^{N_{\tilde{s}}} \epsilon_{\tilde{s}_{i,f}^{tw}}(p) \tag{1}$$

where $\psi(\cdot)$ denotes the digamma function, $N_{\tilde{s}_{i,f}^{tw}}$ denotes the total number of samples of the signal $\tilde{s}_{i,f}^{tw}(n)$, c_d is the volume of the d-dimensional unit sphere, and d denotes the dimension of the signal $\tilde{s}_{i,f}^{tw}(n)$, and $\epsilon_{\tilde{s}_{i,f}^{tw}}(p)$ is the twice distance between p^{th} sample of the signal and its k^{th} neighborhood.

2.3.2. Time domain features

We used Hjorth parameters, namely, *Activity*, *Mobility*, and *Complexity*. The *Activity* feature calculates the signal power, the *Mobility* the mean frequency, and the *Complexity* the changes in the frequency of the signal $\tilde{s}_{i,f}^{tw}(n)$ [54]. These features can be calculated using.

$$M^{Activity}\left(\tilde{s}_{i,f}^{tw}(n)\right) = var\left(\tilde{s}_{i,f}^{tw}(n)\right)$$

$$M^{Mobility}\left(\tilde{s}_{i,f}^{tw}(n)\right) = \sqrt{\frac{M^{Activity}\left(D\left(\tilde{s}_{i,f}^{tw}(n)\right)\right)}{M^{Activity}\left(\tilde{s}_{i,f}^{tw}(n)\right)}}$$

$$M^{Complexity}\left(\tilde{s}_{i,f}^{tw}(n)\right) = \frac{M^{Mobility}\left(D\left(\tilde{s}_{i,f}^{tw}(n)\right)\right)}{M^{Mobility}\left(\tilde{s}_{i,f}^{tw}(n)\right)} \tag{2}$$

where $D(\cdot)$ represents the first-order forward difference operator. In addition to the Hjorth parameters, extra time-domain features namely, normalized first difference and normalized second difference were used. These features quantify the self-similarity structure of signals [62,77]. The 1st difference feature of the signal segment $\tilde{s}_{i,f}^{tw}(n)$ is calculated as.

$$M^{FD}\left(\tilde{s}_{i,f}^{tw}(n)\right) = \frac{1}{N_{\tilde{s}_{i,f}^{tw}} - 1}\sum_{k=1}^{N_{\tilde{s}}-1}\left|\tilde{s}_{i,f}^{tw}(k+1) - \tilde{s}_{i,f}^{tw}(k)\right| \tag{3}$$

The normalized version of the 1st difference can then be expressed as

$$M^{NFD}\left(\tilde{s}_{i,f}^{tw}(n)\right) = \frac{M^{FD}\left(\tilde{s}_{i,f}^{tw}(n)\right)}{\sigma_{\tilde{s}_{i,f}^{tw}}} \tag{4}$$

where $\sigma_{\tilde{s}_{i,f}^{tw}}$ denotes the standard deviation of $\tilde{s}_{i,f}^{tw}(n)$. The 2nd difference can be calculated as

$$M^{SD}\left(\tilde{s}_{i,f}^{tw}(n)\right) = \frac{1}{N_{\tilde{s}_{i,f}^{tw}} - 2}\sum_{k=1}^{N_{\tilde{s}}-2}\left|\tilde{s}_{i,f}^{tw}(k+2) - \tilde{s}_{i,f}^{tw}(k)\right| \tag{5}$$

The normalized 2nd difference is obtained as

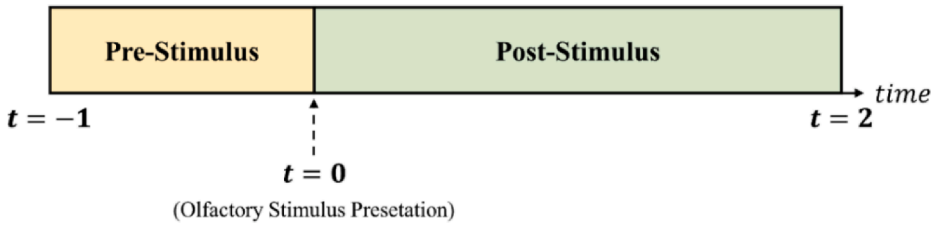

Fig. 1. The timing diagram of the EEG epochs. Each epoch started from the 1000 ms before the stimulus onset ($t = 0$) and lasts up to 2000 ms after the stimulus onset.

$$M^{NSD}\left(\widetilde{s}_{i,f}^{tw}(n)\right) = \frac{M^{SD}\left(\widetilde{s}_{i,f}^{tw}(n)\right)}{M^{FD}\left(\widetilde{s}_{i,f}^{tw}(n)\right)} \tag{6}$$

2.3.3. Filter-Bank common spatial patterns (FBCSP)

We used the filter-bank common spatial patterns method to recognize the subjects with Parkinson's disease from their olfactory EEG responses. During obtaining frequency-specific spatial filters, we used all epochs of the training subjects to calculate the covariance matrices of healthy control (HC) and PD categories. Let $\widetilde{S}_f^{tw}(n) = \begin{bmatrix} \widetilde{s}_{1,f}^{tw}(n) \\ \widetilde{s}_{2,f}^{tw}(n) \\ \vdots \\ \widetilde{s}_{M,f}^{tw}(n) \end{bmatrix}$ represents the M-channel EEG signal. The mean spatial covariance matrices $\Sigma_f^{HC,tw}$ and $\Sigma_f^{PD,tw}$ are calculated using all the training epochs of HC and PD subjects. The frequency-specific spatial filter matrix W_f^{tw} can be constructed using the eigenvectors that maximizing the criterion function $J\left(w_f^{tw}\right)$ expressed as [78,79].

$$J\left(w_f^{tw}\right) = \frac{w_f^{tw^T} \mathrm{P}_f^{D,tw} w_f^{tw}}{w_f^{tw^T} \mathrm{P}_f^{C,tw} w_f^{tw}} \tag{7}$$

where $\mathrm{P}_f^{D,tw}$ and $\mathrm{P}_f^{C,tw}$ denote the frequency-specific discriminative and common activity terms which are obtained as [80].

$$\begin{aligned} \mathrm{P}_f^{D,tw} &= \Sigma_f^{HC,tw} - \Sigma_f^{PD,tw} \\ \mathrm{P}_f^{C,tw} &= \Sigma_f^{HC,tw} + \Sigma_f^{PD,tw} \end{aligned} \tag{8}$$

Here, we selected three eigenvectors from both ends of the eigenvector spectrum ($2m = 6$) as in [80]. We thus obtained spatial filter $W_f^{tw} \in \mathbb{R}^{N_{ch} \times 2m}$ for each frequency band f.

After constructing the frequency-specific spatial filters, for each training subject, the log-variance features of spatially and spectrally filtered the epochs were calculated for each frequency band as.

$$M^{FBCSP}\left(\widetilde{S}_f^{tw}\right) = \log\left(\frac{diag\left(W_f^{tw^T} \widetilde{S}_f^{tw}\ \widetilde{S}_f^{tw^T} W_f^{tw}\right)}{tr\left(W_f^{tw^T} \widetilde{S}_f^{tw}\ \widetilde{S}_f^{tw^T} W_f^{tw}\right)}\right) \tag{9}$$

where the $diag(\cdot)$ function returns the diagonal elements and the $tr(\cdot)$ function returns the sum of the diagonal elements [79].

2.3.4. Brain connectivity

We used linear mutual information to quantify the synchronization (i.e., connectivity) between the signals collected from different brain regions. Briefly, linear mutual information calculates the second-order correlation between signals. For a channel pair (i,j), the linear mutual information can be calculated using [56,61].

$$M^{LinearMI}\left(\widetilde{s}_{i,f}^{tw}(n), \widetilde{s}_{j,f}^{tw}(n)\right) = -\frac{1}{2}\log\left(1 - \left(\rho_{i,j,f}^{tw}\right)^2\right) \tag{10}$$

where $\rho_{i,j,f}^{tw}$ denotes the correlation coefficient of the signals $\widetilde{s}_{i,f}^{tw}(n)$ and $\widetilde{s}_{j,f}^{tw}(n)$.

Note that in the brain connectivity analysis during feature extraction step, we calculated the linearized mutual information of the 600 ms-long signals of the channel pairs indexed by (i,j) for each stimulus segment in the dataset

Note also that we calculated the synchronizations for all ($\frac{64\times63}{2} = 2016$) channel pairs during our analysis.

For entropy and time-domain features, the feature vector ξ^{tw} for any epoch can be obtained as.

$$\xi^{tw} = \begin{bmatrix} \\ \\ M\left(\widetilde{s}_{1,f_1}^{tw}\right) \\ M\left(\widetilde{s}_{2,f_1}^{tw}\right) \\ \vdots \\ M\left(\widetilde{s}_{64,f_1}^{tw}\right) \\ M\left(\widetilde{s}_{1,f_2}^{tw}\right) \\ M\left(\widetilde{s}_{2,f_2}^{tw}\right) \\ \vdots \\ M\left(\widetilde{s}_{64,f_{12}}^{tw}\right) \\ \\ \end{bmatrix} \tag{11}$$

As for the FBCSP method, the log-variance feature vector for any epoch can be obtained as.

$$\xi^{tw} = \begin{bmatrix} M^{FBCSP}\left(\widetilde{S}_{f_1}^{tw}\right) \\ M^{FBCSP}\left(\widetilde{S}_{f_2}^{tw}\right) \\ \vdots \\ M^{FBCSP}\left(\widetilde{S}_{f_{12}}^{tw}\right) \end{bmatrix} \tag{12}$$

And for the linear mutual information method.

$$\xi^{tw} = \begin{bmatrix} M^{LinearMI}\left(\tilde{s}^{tw}_{1,f_1}(n), \tilde{s}^{tw}_{2,f_1}(n)\right) \\ M^{LinearMI}\left(\tilde{s}^{tw}_{1,f_1}(n), \tilde{s}^{tw}_{3,f_1}(n)\right) \\ \vdots \\ M^{LinearMI}\left(\tilde{s}^{tw}_{63,f_1}(n), \tilde{s}^{tw}_{64,f_1}(n)\right) \\ M^{LinearMI}\left(\tilde{s}^{tw}_{1,f_2}(n), \tilde{s}^{tw}_{2,f_2}(n)\right) \\ \vdots \\ M^{LinearMI}\left(\tilde{s}^{tw}_{63,f_2}(n), \tilde{s}^{tw}_{64,f_2}(n)\right) \\ \vdots \\ M^{LinearMI}\left(\tilde{s}^{tw}_{63,f_{12}}(n), \tilde{s}^{tw}_{64,f_{12}}(n)\right) \end{bmatrix} \quad (13)$$

Please note that, after constructing the feature vectors for each epoch, we calculated the average of the feature vectors across all epochs to obtain a unique representative feature vector for each subject. These representative vectors were used for classifier training and test purposes.

In this study, three different classifiers were used in a *leave-one-subject-out* cross-validation framework. The classifiers that we used here are: Fisher's linear discriminant [81], linear and nonlinear support vector machines (SVM) [82]. The kernel size ς of the nonlinear SVM was determined as [56].

$$\varsigma = \sqrt{\frac{1}{L(L-1)} \sum_{i=1}^{L-1} \sum_{j=i+1}^{L} \|\xi_i - \xi_j\|^2} \quad (14)$$

where L is the total number of training feature vectors.

2.4. Proposed classification framework

The operational diagram of the training phase of the classification framework is given in Fig. 2.

In the *EEG Pre-processing* block, first, the EEG signals of each training subject were re-referenced through a CAR filter and then filtered with the filter-bank structure. Next, we extracted the epochs from the filtered EEG signals. In the *Feature Extraction* block, the features were extracted from all channels and all frequency bands for each epoch. These features were then concatenated to form a feature vector for each epoch. Next, in the *Averaging Feature Vector Across Epochs* block, we averaged the feature vectors of all epochs to obtain a unique representative feature vector for each training subject. In the *Classifier Training* block, the representative feature vectors and their respective class information were used to train the classifier for testing purposes.

We presented the flow diagram of the test phase of our framework in Fig. 3. Similar steps in the training phase were performed but the classifier training. Here, in the *Classification* block, we determined the category of the test feature vector by using the trained classifier.

2.5. Comparative analysis

We used linear predictive coding (LPC) [17], wavelet entropy [83], and higher-order spectra [57] as benchmark methods to evaluate the performance of our framework. These methods were previously used to disclose the neural patterns peculiar to the early stage of Parkinson's disease [84]. These benchmark methods were used with slight modifications. For the first method, the EEG signals were filtered into a 2.5–14 Hz frequency band, which elicited the most distinctive spectral characteristics for PD and healthy subjects [17,85]. Before the calculation of LPC features, we used the Akaike information criterion (AIC) to determine the optimum model order [86]. We determined the model order as 12 since most of the channels at each training epoch elicited their minimum AIC value at this model order. The LPC features of each channel were calculated via Burg's method according to the selected model order and then concatenated to form a column feature vector.

The second method is the wavelet entropy analysis which is frequently used in neural activity analysis studies [83,87,88] and PD diagnosis studies [84]. Before the wavelet decomposition, the EEG signals were filtered into 0.5–48 Hz. frequency band. Next, we applied 7-level Haar wavelet decomposition for each channel to extract the

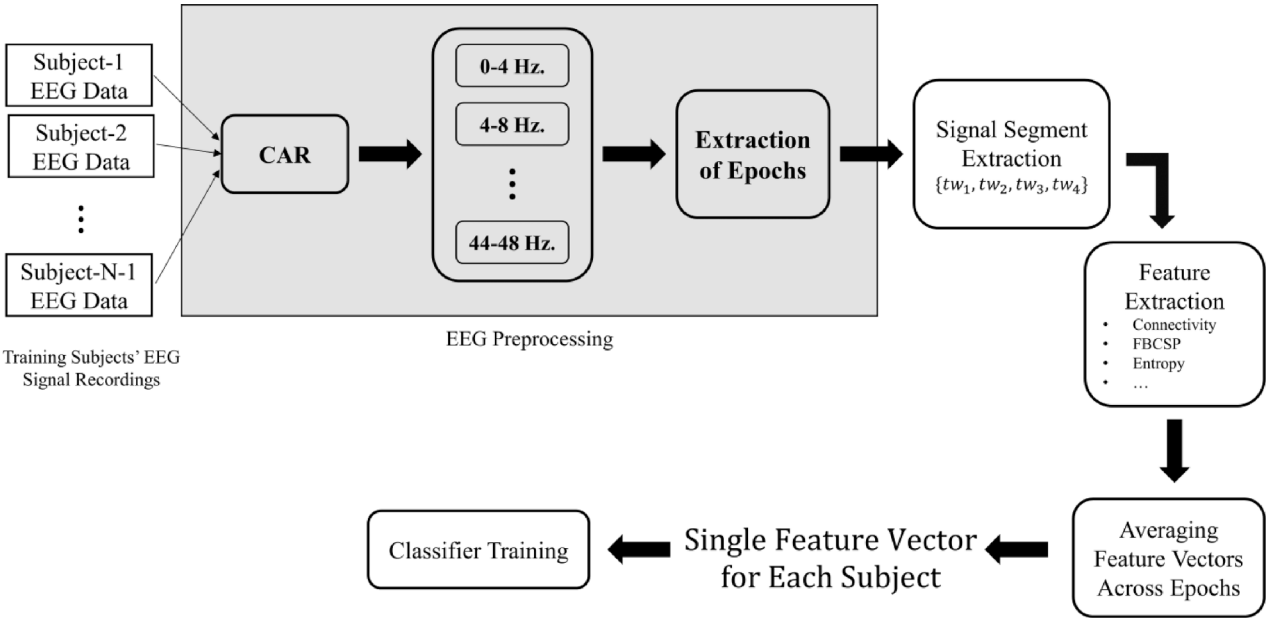

Fig. 2. Operational diagram of the training phase of the classification framework.

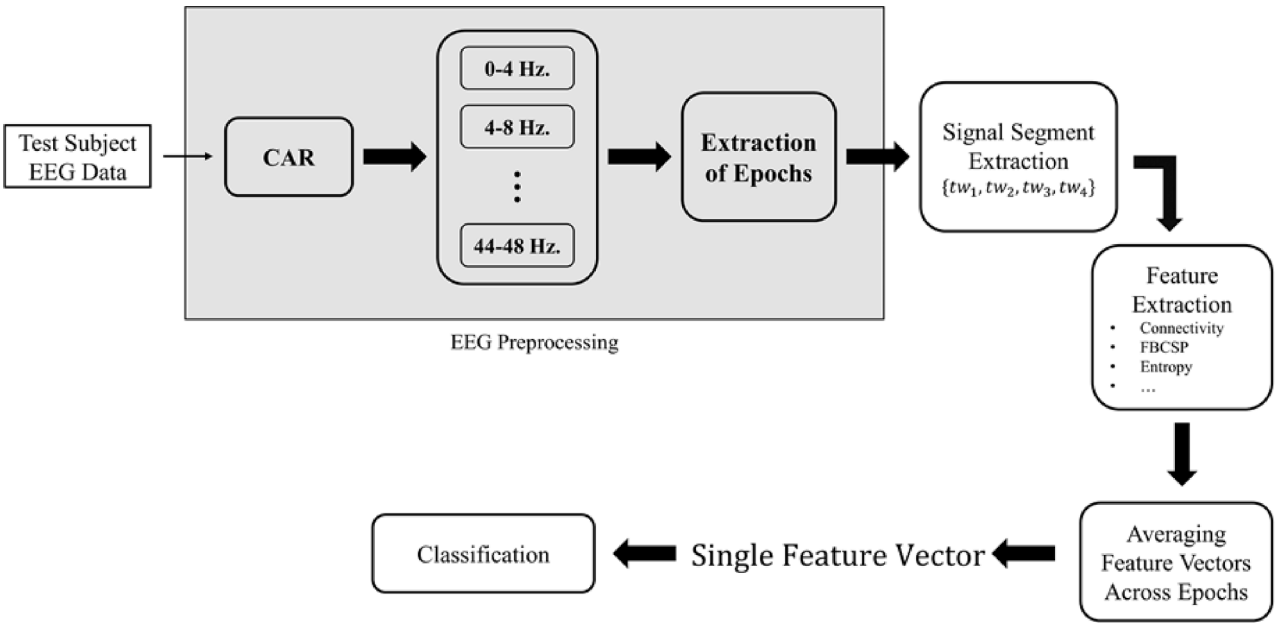

Fig. 3. The flow diagram of the test phase of the classification framework.

dominant physiological EEG rhythms (i.e., δ : 0.5–4 Hz., θ : 4–8 Hz., α : 8–13 Hz., β : 13–30 Hz., and γ : 30–48 Hz.) [63,83]. We used the level-7 approximation (A7), and levels-4, 5, 6, and 7 detail coefficients (D4, D5, D6, and D7) to calculate the wavelet entropy features of each channel. The resulting wavelet entropy-based feature vectors were obtained for each epoch by concatenating all the channel entropies.

The third method calculates the higher-order spectral features from each channel [57]. The EEG signals were initially filtered into 0.5–48 Hz. frequency band through a 4th order Butterworth filter. Next, we used the Hanning window with a length of 0.4 s with %75 overlap to obtain the Fourier spectrum of signals. Then, we calculated the bispectrum of the neural signals using $B(f_1,f_2) = E\{X(f_1)X(f_2)X^*(f_1+f_2)\}$ formula. Here, $B(f_1,f_2)$ denotes the bispectrum calculated for a frequency pair (f_1,f_2), $X(f_1)$ represents the spectral coefficients of the signal $x(t)$ at frequency f_1 , and * indicates the complex conjugate. The bispectrum values for each frequency pair (f_1,f_2) within [0.5 48] Hz. were used to calculate the $H_{logsum}(B(f_1,f_2)) = \sum_{f_1,f_2\in[0.548]}\log|B(f_1,f_2)|$ for each channel [89]. Finally, we concatenated the H_{logsum} values calculated for each channel to form a feature vector for each epoch.

Note that the resulting feature vectors were averaged to obtain a representative feature vector for each subject. For these benchmark methods, we applied feature selection to determine and use the most informative features before the classification analysis.

As a fourth method, we used the subjects' TDI scores, obtained through the Sniffin' Sticks test, for classification purposes. We determined whether the subject has PD or not by comparing their TDI scores with the threshold that was set according to the previous clinical studies [90]. Here, a subject was determined as HC if his/her TDI score indicated a normosmia. On the contrary, if his/her TDI score indicated either hyposmia or anosmia, he/she was determined as PD.

3. Results

In this section, we presented the classification performances as well as biophysical outcomes of the proposed classification framework.

3.1. Performance results

We performed the *leave-one-subject-out* cross-validation to evaluate the characterization performance of each feature extraction method. At each cross-validation cycle, one subject's EEG data were excluded as test set, and data of the remaining subjects were used as training set. In the training phase, we constructed the representative feature vectors for each subject and then, these representative vectors were used to train the classifiers. Next, the data of excluded test subject was used to construct the test feature vector to test the classifier. At each cross-validation cycle, we determined if the classifier correctly identified the category of the test feature vector. Then, the overall classification performance is determined by.

$$\text{Performance}\,(\%) = 100 \times \frac{\#\text{ of correctly classified subjects}}{\#\text{ of total subjects}} \tag{15}$$

Note that we calculated the Fisher ratio of each individual feature across training feature vectors to select the most discriminative features at each cross-validation cycle. The Fisher ratio for the feature indexed by ρ can be calculated as.

$$F(\rho) = \frac{\left|\mu_\rho^{HC} - \mu_\rho^{PD}\right|}{\sigma_\rho^{HC} + \sigma_\rho^{PD}} \tag{16}$$

where μ_ρ^A and σ_ρ^A denotes the mean and standard deviation of the feature calculated across training feature vectors of category $A \in \{HC, PD\}$. Here, *HC* and *PD* represent the healthy control and Parkinson's disease categories. We selected the features which had the Fisher ratio higher than the mean plus two times the standard deviation of the Fisher ratio of all features [91]. The performance results of each different feature extraction method and different time intervals are presented in Figs. 4 and 5 for PEA and CO_2 stimuli, respectively.

The performance results in Fig. 4 show that the entropy and connectivity features extracted from the 100–700 and 200–800 ms temporal segments elicited greater classification accuracies (81.25%) than other feature extraction methods for the PEA stimulus, respectively. Also, the entropy feature attained its maximum subject classification performance (100–700 ms. with linear SVM) earlier than connectivity feature (200–800 ms. with FLD). This timing difference of the maximal performances might be due to the algorithmic differences of linear SVM and FLD classifiers. The sensitivity and specificity values corresponding to the patients and healthy subjects were found as 90% and 66.67% for entropy, and %100 and %76.87 for connectivity features.

As regards the CO_2 stimulus (see Fig. 5), the normalized 1st difference feature elicited 75.86% accuracy in the 100–700 ms time interval for

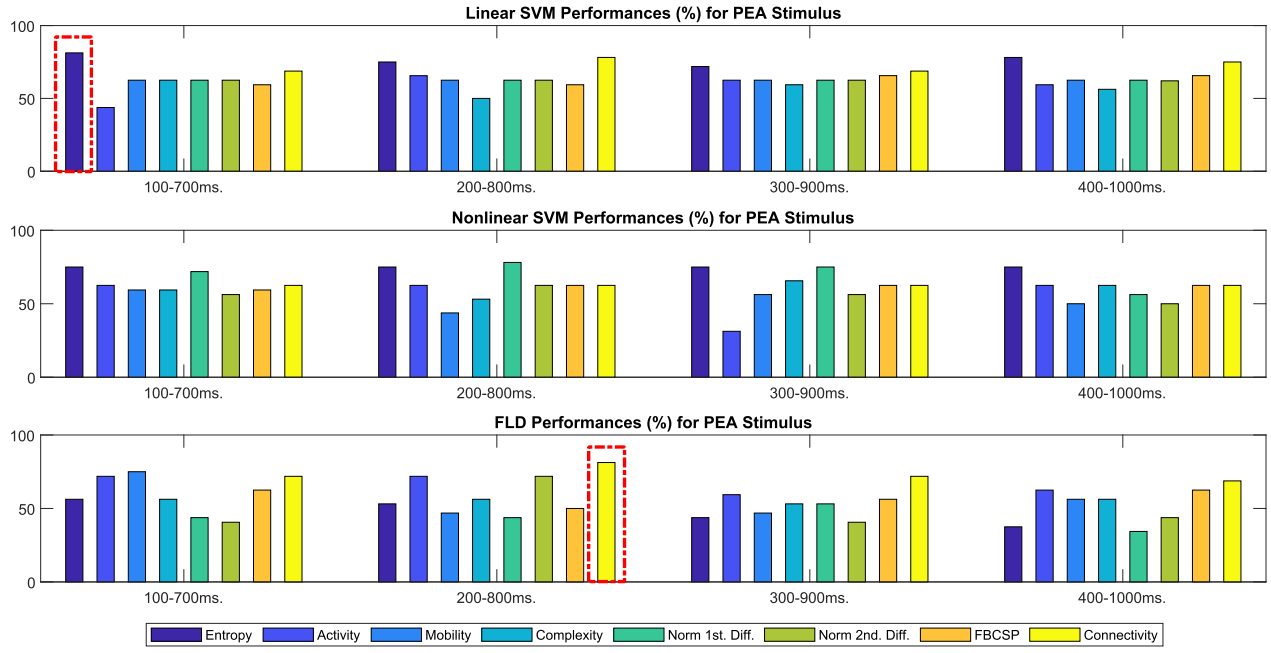

Fig. 4. The recognition performances of our diagnosis framework for PEA stimulus. We adopted *leave-one-subject-out* cross-validation during performance evaluations. We presented the performances for each different time window, feature extraction method, and classifier. The dot-dashed-framed performances indicate the highest ones.

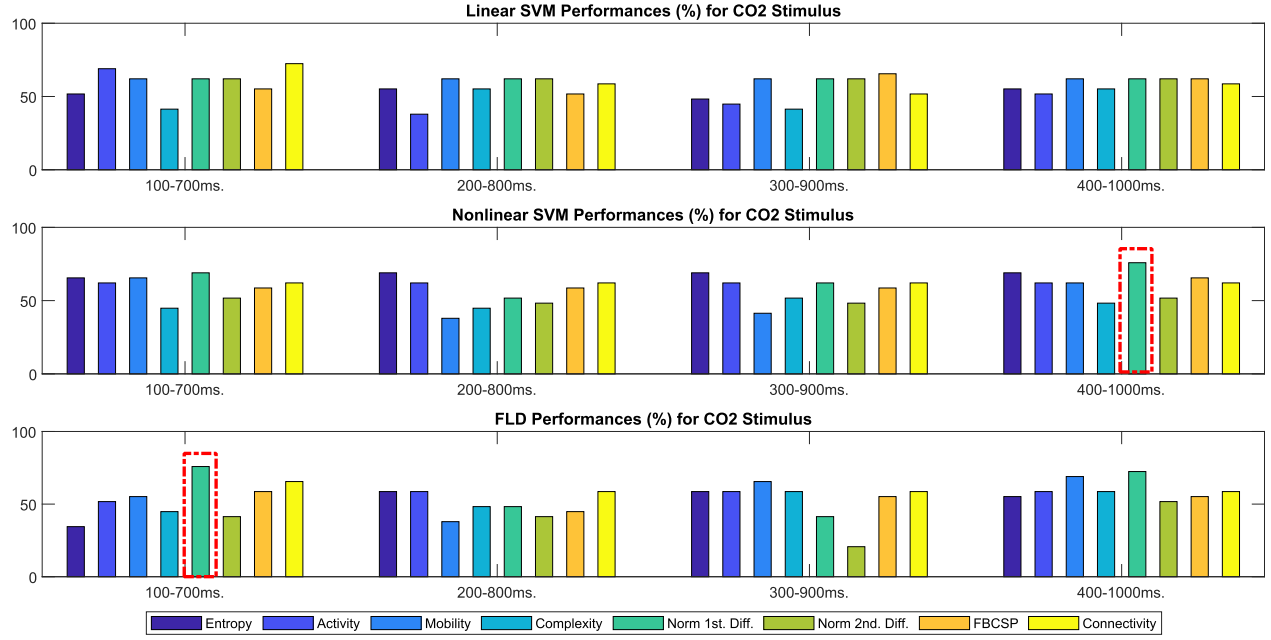

Fig. 5. The recognition performances of our diagnosis framework for CO_2 stimulus. We adopted *leave-one-subject-out* cross-validation during performance evaluations. We presented the performances for each different time window, feature extraction method, and classifier. The dot-dashed-framed performances indicate the highest ones.

FLD and the 400–1000 ms for nonlinear SVM. Besides, the connectivity feature elicited 72.41% performance in the 100–700 ms time interval with linear SVM classifier. The sensitivity and specificity values were 66.67% and 90.91% for the normalized 1st difference feature and 80% and 76.87% for the connectivity feature, respectively. Note that the sensitivity and specificity values for both PEA and CO_2 stimulus were calculated in the condition where the maximum classification performances were achieved. These performances indicate that PEA-induced neural patterns are more informative than CO_2-induced ones in diagnosing subjects with PD.

In our analysis, we decomposed EEG activity into several components via band pass filters with 4 Hz bandwidth since many cognitive,

motor, and sensory events evoke neural processes encapsulated in several frequency bands [92–96]. To further highlight the importance of using a filter-bank structure, we conducted an extra entropy-based classification analysis by excluding the filter-bank structure. To that end, we re-referenced the EEG signals into the common average and filtered the signals (two-pass filtering) into 0.5–48 Hz using a 4^{th} order Butterworth filter. Thereafter, we calculated the entropies of the PEA-induced EEG signals within 100–700 ms. We averaged the entropy features across trials and then aligned the features according to their Fisher scores and used the first 6, 13, 19, 26, 32, 38, 45, 51, 58, and 64 features for both (with and without using filter-bank) cases. The *leave-one-subject-out* classification performances of three classifiers are presented in Fig. 6. The results in Fig. 6 show that the performances obtained using the filter-bank structure match and exceed the performances obtained without using the filter-bank structure for all different feature vector dimensionalities and classification methods. This suggests that using a frequency-resolved spatio-temporal feature analysis is beneficial in capturing the neuronal pathologies, which were demonstrated to be localized in certain sub-bands rather than distributed across the frequency bands [84,97–99].

3.2. Biophysical results

We determined the channels and respective frequency bands of the frequently selected univariate features (entropy for PEA and normalized 1st difference for CO_2) across all cross-validation cycles. The most frequently selected sixteen channels and their respective frequency ranges were presented in Table 2. Our findings in Table 2 show that the frequently selected entropy feature was mainly obtained from right central (C2) and right frontocentral (FC2) channels for the PEA stimulus. For the C2 channel, the frequently selected entropies calculated from the spectrum consists of the entire sub-bands except for the alpha band (8–12 Hz.). As for the FC2 channel, entropy of beta (20–24 Hz. and 24–28 Hz.) and gamma (36–40 Hz., 40–44 Hz., 44–48 Hz.) band EEG signals were the most frequently selected features among others.

Table 2
The frequently used entropy and normalized 1st difference features of sixteen channels and their respective frequency bands for olfactory (PEA) and trigeminal (CO_2) stimuli. The left and right sides of this table provide the channels and respective frequency bands of entropy and normalized 1st difference features for PEA and CO_2 stimulation, respectively. Both entropy and normalized 1st difference features were obtained from the neural activity in 100–700 ms time interval.

PEA Stimulation (Entropy → 81.25%)		CO_2 Stimulation (Normalized 1st Difference → 75.86%)	
Channels (Freq. Bands) (100–700 ms)		Channels (Freq. Bands) (100–700 ms)	
C2 (0–4 Hz.)	C2 (28–32 Hz.)	TP8 (4–8 Hz.)	P4 (4–8 Hz.)
C2 (4–8 Hz.)	C2 (32–36 Hz.)	F4 (4–8 Hz.)	P6 (4–8 Hz.)
C2 (12–16 Hz.)	C2 (36–40 Hz.)	F8 (4–8 Hz.)	AF7 (4–8 Hz.)
C2 (16–20 Hz.)	FC2 (36–40 Hz.)	FT7 (4–8 Hz.)	FPz (4–8 Hz.)
C2 (20–24 Hz.)	C2 (40–44 Hz.)	F3 (4–8 Hz.)	O1 (36–40 Hz.)
FC2 (20–24 Hz.)	FC2 (40–44 Hz.)	Fp2 (4–8 Hz.)	P8 (36–40 Hz.)
C2 (24–28 Hz.)	C2 (44–48 Hz.)	F7 (4–8 Hz.)	FC4 (36–40 Hz.)
FC2 (24–28 Hz.)	FC2 (44–48 Hz.)	Fp1 (4–8 Hz.)	C3 (36–40 Hz.)

The frequently selected normalized 1st difference features, which were found within theta (4–8 Hz.) and gamma (36–40 Hz.) bands for CO_2 stimulation, revealed that the discriminative channels were distributed throughout the brain regions, unlike the PEA stimulus case.

We also performed the similar analyses for the linear mutual information (bivariate) method. The results of this analysis presented in Table 3 show that the statistical interactions between frontal, temporal,

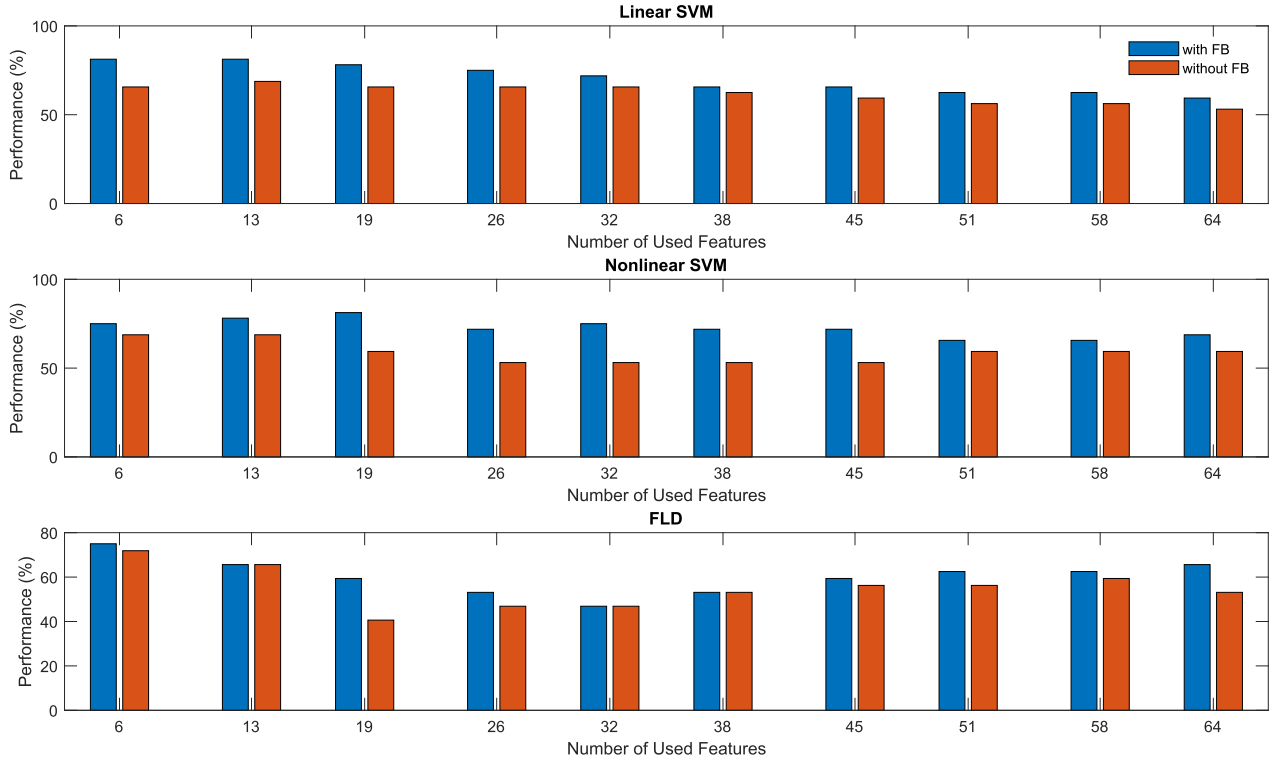

Fig. 6. The classification performances for both with and without using the filter-bank (FB) structure for PEA stimulus. The blue and red bars indicate the performances with and without using the filter-bank structure, respectively. We used different number of features while evaluating the performance. Note that this classification analysis was performed using the neural features calculated by the Kozachenko-Leonenko entropy estimator of the electrophysiological signals only from 100 to 700 ms time interval. The upper part of the figure represents the performances of linear SVM, the middle the nonlinear SVM, and the lower the FLD method.

Table 3
The frequently used linear mutual information features of sixteen channel pairs and their respective frequency ranges for olfactory (PEA) and trigeminal (CO_2) stimuli. The left and right sides of this table provide the channel pairs and respective frequency bands of linear mutual information features for PEA and CO_2 stimulation, respectively. Note that the features were obtained from the neural activity in 200–800 ms and 100–700 ms time interval for PEA and CO_2 stimuli, respectively. We also provided these connectivity patterns graphically (please see Supplementary Fig. 3).

PEA Stimulation (81.25%)		CO_2 Stimulation (72.41%)	
Channel Pairs (Freq. Bands) (200–800 ms.)		Channel Pairs (Freq. Bands) (100–700 ms.)	
FC5-P5 (0–4 Hz.)	P5-T7 (0–4 Hz.)	F2-FC1 (44–48 Hz.)	T7-P8 (24–28 Hz.)
FT7-T7 (24–28 Hz.)	P8-Oz (36–40 Hz.)	FC5-Cz (40–44 Hz.)	FC1-CP4 (44–48 Hz.)
TP7-O1 (4–8 Hz.)	AF7-FT8 (28–32 Hz.)	FT8-T8 (24–28 Hz.)	FC3-Cz (40–44 Hz.)
P3-P4 (0–4 Hz.)	AF7-PO5 (40–44 Hz.)	FT8-O2 (24–28 Hz.)	CP5-T7 (40–44 Hz.)
P5-F3 (0–4 Hz.)	PO6-FT8 (40–44 Hz.)	FT7-CPz (40–44 Hz.)	FC5-C3 (40–44 Hz.)
TP7-T8 (32–36 Hz.)	FP2-FC4 (16–20 Hz.)	P5-FT8 (24–28 Hz.)	F1-Cz (40–44 Hz.)
P5-FCz (0–4 Hz.)	AF7-PO4 (40–44 Hz.)	C1-F3 (40–44 Hz.)	FC6-FC3 (8–12 Hz.)
F8-CP3 (0–4 Hz.)	T8-TP8 (16–20 Hz.)	FT7-P3 (40–44 Hz.)	FCz-CPz (44–48 Hz.)

and central brain regions are mostly occurred at gamma frequency range for both PEA and CO_2 stimulation cases.

The results in Figs. 4 and 5 showed that the PEA stimulation elicited better subject discrimination performance than that of the CO_2 stimulus for both entropy and linear mutual information methods. To that end, we first calculated the entropy and synchronization feature vectors for each subject. Then, we performed a statistical *t*-test analysis between the features of healthy control and PD subjects for PEA stimuli. The *P*-values in Table 4 shows that all the frequently selected entropy and linear mutual information features appeared as statistically significant. Please note that none of these features reached the significance level ($P_{FDR} < 0.05$) when we carried out the Benjamini-Hochberg (B-H) method for correcting multiple comparison problems [100]. This may be due to an insufficient number of subjects used in this study.

Table 4
The uncorrected *P*-values of the entropy and linear mutual information features. The left and right sides of this table provide the *P*-values obtained by comparing the entropy and linear mutual information values between control subjects and subjects with Parkinson's disease, respectively. The time window of 100–700 ms was selected for the entropy and 200–800 ms for the linear mutual information methods. Odorant stimulation was PEA for which the maximum discrimination (81.25%) was obtained for both feature extraction methods.

Entropy (100–700 ms.)		Linear Mutual Information (200–800 ms.)	
Channel (Freq. Band)	*P*-Value	Channel Pair (Freq. Band)	*P*-Value
C2 (0–4 Hz.)	0.0227	FC5-P5 (0–4 Hz.)	2.1×10^{-6}
C2 (4–8 Hz.)	0.0080	FT7-T7 (24–28 Hz.)	2.83×10^{-6}
C2 (12–16 Hz.)	0.0051	TP7-O1 (4–8 Hz.)	6.7×10^{-6}
C2 (16–20 Hz.)	0.0039	P3-P4 (0–4 Hz.)	1.4×10^{-5}
C2 (20–24 Hz.)	0.0023	P5-F3 (0–4 Hz.)	1.8×10^{-5}
FC2 (20–24 Hz.)	0.0150	TP7-T8 (32–36 Hz.)	4.71×10^{-5}
C2 (24–28 Hz.)	0.00141	P5-FCz (0–4 Hz.)	4×10^{-5}
FC2 (24–28 Hz.)	0.012	F8-CP3 (0–4 Hz.)	1.59×10^{-4}
C2 (28–32 Hz.)	0.0013	P5-T7 (0–4 Hz.)	1.34×10^{-4}
C2 (32–36 Hz.)	9.71×10^{-4}	P8-Oz (36–40 Hz.)	4.71×10^{-5}
C2 (36–40 Hz.)	0.0012	AF7-FT8 (28–32 Hz.)	1.23×10^{-4}
FC2 (36–40 Hz.)	0.02	AF7-PO5 (40–44 Hz.)	5.5×10^{-5}
C2 (40–44 Hz.)	7.55×10^{-4}	PO6-FT8 (40–44 Hz.)	2×10^{-4}
FC2 (40–44 Hz.)	0.02	FP2-FC4 (16–20 Hz.)	9.61×10^{-5}
C2 (44–48 Hz.)	6.18×10^{-4}	AF7-PO4 (40–44 Hz.)	7.3×10^{-5}
FC2 (44–48 Hz.)	0.0157	T8-TP8 (16–20 Hz.)	1.44×10^{-4}

3.3. Benchmark performance comparison results

The performance comparison results of the electrophysiological and clinical benchmark methods are given in Table 5. The results show that our entropy-based framework elicited the same performance with wavelet entropy method and outperforms the LPC method for the PEA stimulus case.

As for CO_2, our framework exceeded the performance of the wavelet entropy method, however, the performance of LPC and Sniffin' Sticks-based discrimination methods slightly exceeded the performance of our framework. The sensitivity and specificity values of TDI scores were calculated as 50% and 95%, respectively. It means that TDI scores could not discriminate the healthy controls reliably. The performance of the bispectrum-based method remained modest.

4. Discussion

The neuroelectrical responses of the brain to chemosensory stimuli involve many complex neuronal processes [101,102]. Deciphering these complex processes requires advanced mathematical analysis methods [5,103]. Most of the PD versus HC discrimination studies utilize salient features from resting-state and cognitive/motor task-based experiments [5,7,17,57,60,104]. These studies achieved remarkable discrimination performances by showing considerable changes in neural dynamics in PD patients. However, very few studies have analyzed chemosensory-induced EEG signals in an automatized manner for PD detection purposes so far. The techniques for detecting PD patients are based on analysis of the chemosensory-induced ERP amplitude and latencies, spectrum analysis [49], and global field power analysis [30]. In this study, we suggest that investigating the spatial, spectral, and temporal characteristics of the chemosensory-induced brain activity may provide crucial information about complex neuronal activation/communication dynamics [63]. In that context, the chemosensory-induced EEG signals were characterized by several features to identify healthy subjects and subjects with Parkinson's disease. We evaluated the characterization performances of these features in a leave-one-subject-out cross-validation scheme. The discussion related to the performances and biophysical findings is below.

4.1. Performance analysis

The results in Fig. 4 show that using PEA stimulus resulted in

Table 5
Performance comparison with benchmark methods. We used the leave-one-subject-out cross-validation procedure when obtaining the performances. The second and third row of the table provides the performances (%) obtained for PEA and CO_2 stimulations, respectively. The last column shows the classification result using the TDI scores of the subjects.

Used Stimulus	Proposed Framework	Linear Predictive Coding [17]	Wavelet Entropy [83]	Bispectrum-based [57]	TDI Scores (Sniffin' Sticks')
PEA	81.25% (Entropy, 100–700 ms)	75% (200–800 ms)	81.25% (400–1000 ms)	71.87% (100–700 ms)	78.13%
CO_2	75.86% (Norm 1st Diff., 100–700 ms)	79.31% (100–700 ms)	65.51% (100–700 ms)	72.41% (200–800 ms)	

improved detection of subjects with Parkinson's disease (PD) from electrophysiological signals when using entropy and linear mutual information used for feature extraction. Specifically, our analysis revealed significantly higher values of EEG entropy within the 100–700 ms interval, as well as higher brain connectivity within the 200–800 ms interval, among healthy individuals exposed to the PEA stimulus when compared with PD subjects (refer to Supplementary Figs. 1 and 2). These observations state that the entropic separability of neural signals evoked by PEA may signify alterations in the nonlinear dynamical characteristics of neural activity, and a decline in connectivity suggests an attenuated olfactory information processing due to PD [27,29,46,97,105]. Furthermore, when considering the PEA stimulus, the outcomes presented in Table 5 indicate that the wavelet entropy measure demonstrated comparable performance to our framework in classifying PD subjects and healthy individuals.

As regards the CO_2 stimulus (please see Fig. 5), the normalized 1st difference feature derived from the 100–700 ms interval after the stimulus onset exhibited superior performance when compared with other methods. This finding suggests that the mean of instantaneous changes in the amplitude of EEG activity resulting from trigeminal stimulation plays a crucial role in determining the subjects' neurological conditions. Furthermore, when comparing the performance of our framework with benchmark methods for the CO_2 stimulus, it is worth noting that the linear predictive coding method displayed slightly better performance than our framework.

The performance results of power-based (i.e., variance-based) methods such as FBCSP, Activity, Mobility, and Complexity, as presented in Figs. 4 and 5, indicate their limitations in capturing the alterations associated with Parkinson's disease (PD), unlike entropy- and connectivity-based methods. These performance disparities highlight that relying solely on the oscillatory power of EEG activity is insufficient to determine whether individuals are affected by PD [5,48,99,106–108]. This observation suggests that entropy and connectivity analysis methods can potentially reveal the underlying dynamical structure of brain activity that cannot be unveiled by second-order signal characteristics [5].

In a broader context, the EEG signals triggered by the PEA stimulus exhibited more distinct features that facilitated the diagnosis of PD, aligning with previous literature [37]. This notable separability may underscore the impairment of the olfactory information processing mechanism in PD, including the reduced volume of the olfactory bulb [71,109,110]. Consequently, PD-related deterioration primarily affects the dynamics of olfactory information processing rather than trigeminal information processing.

Psychophysical tests have demonstrated that trigeminal sensitivity mainly remains intact in individuals with Parkinson's disease (PD) [44,111]. This indicates that evaluating the trigeminal sensation through psychophysical tests alone is not useful for identifying PD subjects. Despite the preserved characteristics of the trigeminal system, our framework based on electrophysiological feature extraction successfully extracted discerning features from CO_2-induced EEG signals, enabling the detection of PD subjects. These features can be a supportive tool for determining whether individuals have PD.

The electrophysiological dynamics induced by a PEA stimulus are reliable for diagnosing PD patients, according to the obtained sensitivity and specificity values, whereas CO_2-induced neural activity showed accurate detection of healthy control subjects. Furthermore, we found that TDI scores could diagnose PD but could not identify healthy control participants. According to these results, olfactory stimulation evokes electrophysiological patterns that contain information regarding brain alterations due to Parkinson's disease.

When the number of features is much larger than the number of samples, likewise in our study, overfitting becomes a significant concern. To mitigate this problem, we applied a Fisher ratio based feature selection to identify the most informative feature subset to attenuate the overfitting prior to the classification [112,113].

We also tested the reliability and generalizability of our framework by using a *leave-one-subject-out* cross validation scenario, which is widely adopted for testing against overfitting [114,115]. Both our classification and sensitivity–specificity performances given in the *Results* section indicated that our framework achieved considerable success in diagnosis of PD.

Nevertheless, a larger dataset is required to assess the model's robustness and usefulness in which we raised this issue in the "Limitation of Study" section to encourage further research to address in this direction.

4.2. Using independent component analysis (ICA) as Pre-Processing

The ICA method, which we did not incorporate in our framework, maybe a crucial alternative to reveal the underlying latent dynamics from the EEG signals with poor spatial resolution [116,117]. The poor resolution and artifacts of EEG signals posits that the extracted information from the activity is lesser than it should be. Our performances, as well as biophysical results, highlights that our framework can unravel chemosensory-induced EEG dynamics to a great extent.

To show how ICA affect the diagnosis performance of our framework, we applied the KMAR algorithm [118] as preprocessing, which automatically finds and removes the artifacts from EEG signals with the help of ICA. During our analysis, we performed the same algorithmic steps to our stimulus epochs, as illustrated in Algorithm-1 in [118]. We selected entropy and connectivity as feature extraction methods and also PEA as odorant stimulus during evaluation since this combination provided outperforming diagnosis performance.

The performance results are presented in Table 6. These performances suggest that while the ICA-based preprocessing (artifact rejection) could improve the PD diagnosis accuracy of our entropy-based framework, the diagnostic performance remains the same for the brain connectivity-based framework.

Another significant observation from Table 6 is that the temporal dynamics elicited after ICA-based artifact removal are somewhat different than that of the EEG signals without artifact rejection since the time intervals of maximal performances are slightly different from each other. Considering these two outcomes , using ICA for our entropy-based PD diagnosis framework seems beneficial, albeit with a computational cost.

4.3. Using linearized mutual information for brain connectivity analysis

To assess the synchronization between EEG channels, we used the linearized mutual information approach [61,119]. This method utilizes the correlation coefficient for calculating the inter-channel synchronization. Previous research has demonstrated the successful application of linear methods in characterizing the interaction dynamics of brain activity [56]. Moreover, linear methods have been preferred in various studies due to their practicality and computational efficiency [120].

It is important to acknowledge that the intrinsic nonlinear dynamics of brain activity may lead to the oversight of higher-order statistical correlation terms when employing simple linear correlation methods for

Table 6
The performances obtained using ICA and without ICA.

Methods		Performances (%) (using PEA as odorant)
Without ICA (our framework)	Entropy	81.25% (achieved at 100–700 ms)
	Connectivity	81.25% (achieved at 200–800 ms)
With ICA [118]	Entropy	84.38% (achieved at 200–800 ms)
	Connectivity	81.25% (achieved at 200–800 ms)

calculating the inter-channel synchronizations. In such circumstances, using generalized correlation calculation methods, such as mutual information [121–123] or correntropy [124,125], may prove advantageous when they are used with linear methods [123]. Nonetheless, our findings reveal that the linearized mutual information attained a classification accuracy of 81.25%. This suggests that, to some extent, the assumption of linear correlation between EEG channels can unveil distinctive synchronization patterns between healthy controls and PD, particularly in the presence of chemosensory stimuli.

4.4. Biophysical findings

The frequently selected features were provided in Tables 2 and 3 for entropy and connectivity methods, respectively. The entropy features extracted from the right frontocentral and central regions were consistently selected for classification at each cross-validation cycle. These two regions, which play a crucial role in motor-related functions, strongly interact with the left putamen. It was previously shown that olfactory bulb volume, which is used as an indicator of proper olfactory functioning [110], strongly correlated with the volume of the left putamen [126]. It may be possible that the altered functionality of the left putamen disrupts the neural information processing mechanism during olfaction and during other cognitive, sensory, and motor tasks [99,127,128]. This suggests that reduced olfactory performance can be correlated with the deterioration of neural activities of motor-related structures [32,129]. Considering all these biophysical findings, the change in neural activity characteristics in motor-related areas parallel to the abnormalities in olfactory-related areas is not surprising. The entropy changes in these two regions have been considered as a potential marker caused by PD, which may explain the sensory-related cortical network degeneration [99].

Furthermore, the right central and frontocentral electrodes mostly reflect the electrical activity of the right medial frontal gyrus and right angular gyrus, which take place in default mode network operations [130], attention re-orientation towards top-down processing [131], and multisensory information integration [30]. The olfactory information processing relies on the top-down processes [132], which emerged as the suppression of the default mode network [133]. The altered neural activity patterns of these regions reflect the deterioration of attention- and default-mode network-related processes due to PD which may indicate deteriorated chemosensory information processing mechanism. Furthermore, the consistently selected central and frontocentral channels were right-lateralized which may be due to asymmetric dopamine levels due to PD [30].

Besides the right central and frontocentral regions, our feature selection analysis selected the left parietal, temporal, and right frontal regions, which are known to participate in motor- and sensory-related functions, with slightly reduced observation frequencies in PEA stimulus case [134–136]. These regions have also been demonstrated to involve in olfactory-stimulus-related information processing [137].

The connectivity patterns in Table 3 indicate the importance of the left parietal and frontal brain regions for PEA stimulus. It was previously shown that some regions of the left hemisphere participate in a functional network that plays a crucial role in many sensory, emotional, and cognitive processes [138–140]. This suggests that olfactory dysfunction in PD is due to disruption in the functional connectivity among these regions.

The connectivity patterns observed for PEA stimuli predominantly emerged in delta and gamma bands. Besides, the frequently selected connectivity patterns for CO_2 stimuli were mainly in the gamma band. The gamma-band neural activity has been shown to carry important information about the identity of the chemosensory stimuli [63,74,141]. The connectivity patterns in the delta band could classify PD and HC subjects [49,142–144].

As for the CO_2 stimulus case, the frequently selected normalized first difference features were mainly related to the right and left frontal, left temporal, right parietal, and left central regions. Previous studies showed that trigeminal stimulation activates these cortical regions [145].

Given the presented biophysical outcomes, our findings may raise doubts that the biophysical results presented above mainly arise from PD subjects' resting or postural tremors since previous studies have pointed to significant cortico-muscular coherence at the frequency range mainly between 8 and 12 Hz. [146,147]. In addition, some studies argued that the cortical activity within the β frequency range presumably reflects the resting tremor [84,148]. Notwithstanding, our results from the PEA stimulus show that the significant entropy features were derived from a wide range of frequency bands, excluding only the 8–12 Hz band. We show in Table 2 that our CO_2-induced results are related to 4–8 Hz and 36–40 Hz band activities. If the tremor-dominant situation were the case, both α and β frequency-dominant features would be apparent in both PEA and CO_2 results. Besides, considering the findings of previous studies [147,149], observing tremor-related cortical activity within a wide frequency range and the cortical area is impossible. All in all, the obtained significant features could not entirely relate to tremor-related cortical activity.

4.5. Importance of using Chemosensory-Induced EEG signals

This study aimed to evaluate the possible difference in chemosensory-induced neural patterns between PD and HC subjects since olfaction-based diagnosis can be more suitable for elderly participants who could not attend intense cognitive or physical experiments [73]. Here, our classification performances indicate that successful subject discrimination is possible using the chemosensory-induced EEG patterns extracted via BCI feature extraction methods. This may open a new avenue for developing advanced analysis methods to detect PD from olfactory-related neural disruptions [49,150]. Another merit of using chemosensory-induced EEG signals rather than rest-state EEG signals is that the subjects could perform several cognitive tasks during the resting state, which may influence the reliability of the PD detection framework [151]. The cognitive actions performed by subjects during the resting state may influence neural patterns and hinder PD detection accuracy. Another critical point of using chemosensory-induced EEG signals is diagnosing the PD subjects before other symptoms emerge. In a resting state *de novo* PD diagnosis study, it was mentioned that bivariate (inter-channel connectivity) changes appear earlier than univariate changes in *de novo* PD cases [48]. Contrary to this, we showed that chemosensory stimulation evokes critical patterns that can be captured by entropy and normalized 1^{st} difference features. Most PD-related studies use the diagnosed and medicated subjects to demonstrate the validity of their methods. The current study used *de novo* PD subjects who were newly diagnosed and not medicated.

4.6. Limitations of the study

Here, we studied a classification approach that extracts and uses the features from chemosensory-induced EEG oscillations to classify PD and healthy subjects. We evaluated the classification ability of each different feature type extracted from different 600 ms-long time segments. The performance obtained for the PEA stimuli showed that as linear mutual information and entropy methods elicited the maximal recognition performances, the other methods did not. This performance difference among the methods may be due to the insufficient sample size since each method require a different number of samples for an accurate brain activity characterization [152].

In this study, we assume that the discriminating features emerge and vanish at the same time interval for each channel and frequency band. In our previous connectivity-based study [56], we demonstrated that the initiation and duration parameters of activity-specific short-lived synchronizations vary dramatically for each different EEG channel pair. Our classification performances may be improved by finding the optimum

time interval for each channel and frequency band.

Another possible limitation of this study was the number of healthy and PD subjects and the number of epochs collected from each subject. Our approach should be validated in participant groups with larger sizes as well as in prospective studies to capture the possible PD patients from the data bank of idiopathic olfactory dysfunction.

We used four different 600 ms-long time windows to calculate the features from chemosensory-induced EEG signals. A similar time window-based ERP analysis approach was used in [75]. In that study, the authors stated that the significant peaks emerged between 200 and 800 ms temporal region. It may be possible to obtain more significant neural patterns and improved recognition performances by evaluating different temporal regions after the stimulus onset.

In addition, we used spectrally non-overlapping twelve band pass filters with 4-Hz bandwidth, which means we analyzed the stimulus-induced EEG signals with a relatively coarse frequency resolution. Using more advanced and finer spectral decomposition methods could allow the extraction of more informative PD-related patterns from neural activities [153,154].

5. Conclusions

In clinical research, there is a strong interest in identifying reliable biomarkers for diagnosing Parkinson's disease. Assessing the olfactory functioning of subjects using clinical tools is a common approach to reveal their neurological states, although these tests can be biased due to subjective evaluation (rater-dependency) [155]. Alternatively, electrophysiological methods have been proven to be effective in evaluating neurological health.

Many electrophysiology data analysis studies focus on analyzing resting-state EEG activity to identify specific patterns associated with Parkinson's disease for diagnosis [156]. However, the diagnostic accuracy of Parkinson's disease using EEG features during the resting state may be compromised due to potential interference from subjects' cognitive processes or variations in their sleepiness/wakefulness. Another approach involves evaluating electrophysiological features while individuals engage in walking or pedaling experiments [157]. However, capturing physical impairments associated with Parkinson's disease poses a challenge, as motor symptoms typically appear in the later stages of the disease.

In the context of Parkinson's disease (PD), one of the initial functional impairments observed is a decline in olfactory function [158]. Accordingly, our primary goal is to design a robust framework for an accurate diagnosis of Parkinson's disease by evaluating the subjects' neurological condition and capturing the key patterns from chemosensory-induced neural activities. In our framework, in addition to the spatial and spectral analysis used in most EEG-based studies [159,160], we incorporate a time-resolved EEG analysis [159,160] using short-lived sliding time windows. This approach allows us to better capture the PD-related patterns encapsulated in the EEG activity induced by chemosensory stimuli.

We performed subject discrimination utilizing well-known EEG signal features extracted from chemosensory-induced neural activities. Our results indicate that entropy and connectivity features calculated within specific time intervals (100–700 ms and 200–800 ms) are more effective in classifying Parkinson's disease versus healthy subjects when the PEA stimulus is used. However, the discrimination performance is slightly lower for CO_2, possibly due to intact trigeminal sensitivity in Parkinson's disease subjects [45].

Detecting early signs of Parkinson's disease is a challenging yet essential task. Our performance and biophysical results highlight that olfactory stimulation evokes brain patterns containing critical information about the subjects' neurological condition. From this perspective, our study represents an initial step towards the early diagnosis of Parkinson's disease by utilizing chemosensory-induced EEG signals to determine the altered neural patterns resulting from impaired olfactory functioning. The proposed approach can be an alternative or supportive avenue to current clinical approaches to early PD diagnosis [161–163].

In our framework, we assumed that each brain region and frequency band react to chemosensory stimulus simultaneously and isochronously, presumably not the actual case [159]. For the follow-up study, we are studying a robust PD diagnosis framework that captures the latency and duration of chemosensory-induced EEG responses in each brain region and frequency band for improved discrimination between Parkinson's disease and healthy control participants. Additionally, we consider incorporating deep learning strategies as classification methods into our chemosensory-based diagnosis framework.

Our study evaluated various feature extraction methods to characterize impairments in olfactory stimulus-induced EEG signals [56,164]. Functional connectivity and entropy analysis provided valuable insights into the functionality and configuration of brain networks during olfactory stimulation, likely encapsulating distinctive patterns associated with neurological diseases. Tracking the evolution of these patterns through longitudinal experiments can offer insights into disease progression and the likelihood of developing Parkinson's disease. Advanced spatial–temporal information fusion and prediction techniques, such as graph convolutional networks [165] and LSTM models [166,167], could enable the prediction of disease development by analyzing longitudinal EEG data.

In summary, the novelties of our study are as follows:

- We propose a framework that evaluates the subjects' neurological condition or Parkinson's disease diagnosis using chemosensory stimulus-induced EEG signal features, providing a more objective evaluation than clinical assessment and a more robust evaluation than amplitude and latency analysis of CSERP.
- To our knowledge, this is one of the first studies to extract electrophysiological features by using olfactory and trigeminal stimulation to diagnose Parkinson's disease.
- Diverging from existing analysis approaches, we analyze chemosensory-induced EEG oscillations using short-lived sliding time windows to determine which time segments after chemosensory stimulation contain more informative signatures for Parkinson's disease diagnosis.

CRediT authorship contribution statement

B. Orkan Olcay: Conceptualization, Methodology, Investigation, Visualization, Data curation, Formal analysis, Software, Supervision, Validation, Writing – original draft, Writing – review & editing. **Fatih Onay:** Methodology, Formal analysis, Software, Validation, Writing – original draft, Writing – review & editing. **Güliz Akın Öztürk:** . **Adile Öniz:** Supervision, Project administration, Resources. **Murat Özgören:** Supervision, Project administration, Conceptualization, Writing - review & editing .. **Thomas Hummel:** Supervision, Conceptualization, Writing – review & editing. **Çağdaş Güdücü:** Conceptualization, Writing – original draft, Writing – review & editing.

Declaration of Competing Interest

The authors declare that they have no known competing financial interests or personal relationships that could have appeared to influence the work reported in this paper.

Data availability

The authors do not have permission to share data.

Acknowledgement

This study was supported by a grant awarded to Dr. Adile Öniz by the Dokuz Eylül University, Department of Scientific Research Projects with

a grant number 2012.KB.SAG.083. Also, Dr. B. Orkan Olcay is financially supported by the project with grant number 121E122, which was awarded to Dr. Bilge Karaçalı by The Scientific and Technological Research Council of Turkey (TUBITAK).

Appendix A. Supplementary data

Supplementary data to this article can be found online at https://doi.org/10.1016/j.bspc.2023.105438.

References

[1] R. McMackin, P. Bede, N. Pender, O. Hardiman, B. Nasseroleslami, Neurophysiological markers of network dysfunction in neurodegenerative diseases, NeuroImage Clin. 22 (2019) 101706.
[2] D.J. Kim, A.R. Bolbecker, J. Howell, O. Rass, O. Sporns, W.P. Hetrick, A. Breier, B. F. O'Donnell, Disturbed resting state EEG synchronization in bipolar disorder: A graph-theoretic analysis, NeuroImage Clin. 2 (2013) 414–423, https://doi.org/10.1016/j.nicl.2013.03.007.
[3] W. Liu, C. Zhang, X. Wang, J. Xu, Y. Chang, T. Ristaniemi, F. Cong, Functional connectivity of major depression disorder using ongoing EEG during music perception, Clin. Neurophysiol. 131 (2020) 2413–2422, https://doi.org/10.1016/j.clinph.2020.06.031.
[4] R. Zheng, Y. Feng, T. Wang, J. Cao, D. Wu, T. Jiang, F. Gao, Scalp EEG functional connection and brain network in infants with West syndrome, Neural Networks. 153 (2022) 76–86, https://doi.org/10.1016/j.neunet.2022.05.029.
[5] C. Lainscsek, M.E. Hernandez, J. Weyhenmeyer, T.J. Sejnowski, H. Poizner, Non-linear dynamical analysis of EEG time series distinguishes patients with Parkinson's disease from healthy individuals, Front. Neurol. 4 DEC (2013) 200, https://doi.org/10.3389/fneur.2013.00200.
[6] J. Xu, J. Zhang, J. Wang, G. Li, Q. Hu, Y. Zhang, Abnormal fronto-striatal functional connectivity in Parkinson's disease, Neurosci. Lett. 613 (2016) 66–71, https://doi.org/10.1016/j.neulet.2015.12.041.
[7] M. Gérard, M. Bayot, P. Derambure, K. Dujardin, L. Defebvre, N. Betrouni, A. Delval, EEG-based functional connectivity and executive control in patients with Parkinson's disease and freezing of gait, Clin. Neurophysiol. 137 (2022) 207–215, https://doi.org/10.1016/j.clinph.2022.01.128.
[8] S. Schippling, S.A. Schneider, K.P. Bhatia, A. Münchau, J.C. Rothwell, S. J. Tabrizi, M. Orth, Abnormal Motor Cortex Excitability in Preclinical and Very Early Huntington's Disease, Biol. Psychiatry. 65 (2009) 959–965, https://doi.org/10.1016/j.biopsych.2008.12.026.
[9] D. Yates, Neurodegenerative disease: Neurodegenerative networking, Nat. Rev. Neurosci. 13 (2012) 288–289, https://doi.org/10.1038/nrn3248.
[10] M.A. Al-Bunyan, Parkinson's disease: Clinical and electrophysiological evaluation, Saudi Med. J. 21 (2000) 72–75.
[11] J. Kim, M. Criaud, S.S. Cho, M. Díez-Cirarda, A. Mihaescu, S. Coakeley, C. Ghadery, M. Valli, M.F. Jacobs, S. Houle, A.P. Strafella, Abnormal intrinsic brain functional network dynamics in Parkinson's disease, Brain. 140 (2017) 2955–2967, https://doi.org/10.1093/brain/awx233.
[12] A.E. Martinez-Nunez, K. Latack, M.S. Kcomt, A. Mahajan, Olfaction and apathy in early idiopathic Parkinson's disease, J. Neurol. Sci. 439 (2022), 120314, https://doi.org/10.1016/j.jns.2022.120314.
[13] C.K. Cramer, J.H. Friedman, M.M. Amick, Olfaction and apathy in Parkinson's disease, Park. Relat. Disord. 16 (2010) 124–126, https://doi.org/10.1016/j.parkreldis.2009.09.004.
[14] A. Singh, R.C. Cole, A.I. Espinoza, A. Evans, S. Cao, J.F. Cavanagh, N. S. Narayanan, Timing variability and midfrontal ~4 Hz rhythms correlate with cognition in Parkinson's disease, Npj Park. Dis. 7 (2021), https://doi.org/10.1038/s41531-021-00158-x.
[15] R.L. Doty, Olfactory dysfunction in Parkinson disease, Nat. Rev. Neurol. 8 (2012) 329–339, https://doi.org/10.1038/nrneurol.2012.80.
[16] M. Gongora, B. Velasques, M. Cagy, S. Teixeira, P. Ribeiro, EEG coherence as a diagnostic tool to measure the initial stages of Parkinson Disease, Med. Hypotheses. 123 (2019) 74–78, https://doi.org/10.1016/j.mehy.2018.12.014.
[17] M.F. Anjum, S. Dasgupta, R. Mudumbai, A. Singh, J.F. Cavanagh, N.S. Narayanan, Linear predictive coding distinguishes spectral EEG features of Parkinson's disease, Park. Relat. Disord. 79 (2020) 79–85, https://doi.org/10.1016/j.parkreldis.2020.08.001.
[18] S. Bhat, U.R. Acharya, Y. Hagiwara, N. Dadmehr, H. Adeli, Parkinson's disease: Cause factors, measurable indicators, and early diagnosis, Comput. Biol. Med. 102 (2018) 234–241, https://doi.org/10.1016/j.compbiomed.2018.09.008.
[19] A. Osman, J. Silas, Electrophysiological Measurement of Olfactory Function, in: Handb. Olfaction Gustation Third Ed., Wiley Blackwell, 2015: pp. 261–278. https://doi.org/10.1002/9781118971758.ch12.
[20] K. Kondo, S. Kikuta, R. Ueha, K. Suzukawa, T. Yamasoba, Age-Related Olfactory Dysfunction: Epidemiology, Pathophysiology, and Clinical Management, Front. Aging Neurosci. 12 (2020), https://doi.org/10.3389/FNAGI.2020.00208/FULL.
[21] C. Tremblay, R. Emrich, A. Cavazzana, L. Klingelhoefer, M.D. Brandt, T. Hummel, A. Haehner, J. Frasnelli, Specific intranasal and central trigeminal electrophysiological responses in Parkinson's disease, J. Neurol. 266 (2019) 2942–2951, https://doi.org/10.1007/s00415-019-09517-4.
[22] M.E. Fullard, B. Tran, S.X. Xie, J.B. Toledo, C. Scordia, C. Linder, R. Purri, D. Weintraub, J.E. Duda, L.M. Chahine, J.F. Morley, Olfactory impairment predicts cognitive decline in early Parkinson's disease, Park. Relat. Disord. 25 (2016) 45–51, https://doi.org/10.1016/j.parkreldis.2016.02.013.
[23] J.W. Park, D.Y. Kwon, J.H. Choi, M.H. Park, H.K. Yoon, Olfactory dysfunctions in drug-naïve Parkinson's disease with mild cognitive impairment, Park. Relat. Disord. 46 (2018) 69–73, https://doi.org/10.1016/j.parkreldis.2017.11.334.
[24] M.E. Fullard, J.F. Morley, J.E. Duda, Olfactory Dysfunction as an Early Biomarker in Parkinson's Disease, Neurosci. Bull. 33 (2017) 515–525, https://doi.org/10.1007/s12264-017-0170-x.
[25] K. Ezzatdoost, H. Hojjati, H. Aghajan, Decoding olfactory stimuli in EEG data using nonlinear features: A pilot study, J. Neurosci. Methods. 341 (2020), 108780, https://doi.org/10.1016/j.jneumeth.2020.108780.
[26] M. Dibattista, S. Pifferi, A. Menini, J. Reisert, Alzheimer's Disease: What Can We Learn From the Peripheral Olfactory System? Front. Neurosci. 14 (2020) https://doi.org/10.3389/fnins.2020.00440.
[27] Y. Wang, H. Wei, S. Du, H. Yan, X. Li, Y. Wu, J. Zhu, Y. Wang, Z. Cai, N. Wang, Functional Covariance Connectivity of Gray and White Matter in Olfactory-Related Brain Regions in Parkinson's Disease, Front. Neurosci. 16 (2022), https://doi.org/10.3389/fnins.2022.853061.
[28] M.J. Sedghizadeh, H. Hojjati, K. Ezzatdoost, H. Aghajan, Z. Vahabi, H. Tarighatnia, N. Ravel, Olfactory response as a marker for Alzheimer's disease: Evidence from perceptual and frontal lobe oscillation coherence deficit, PLoS One. 15 (12) (2020) e0243535.
[29] C. Tremblay, J. Frasnelli, Olfactory-Trigeminal Interactions in Patients with Parkinson's Disease, Chem. Senses. 46 (2021) 1–8, https://doi.org/10.1093/chemse/bjab018.
[30] E. Iannilli, L. Stephan, T. Hummel, H. Reichmann, A. Haehner, Olfactory impairment in Parkinson's disease is a consequence of central nervous system decline, J. Neurol. 264 (2017) 1236–1246, https://doi.org/10.1007/s00415-017-8521-0.
[31] C. Llanos, M. Rodriguez, C. Rodriguez-Sabate, I. Morales, M. Sabate, Mu-rhythm changes during the planning of motor and motor imagery actions, Neuropsychologia. 51 (2013) 1019–1026, https://doi.org/10.1016/j.neuropsychologia.2013.02.008.
[32] V.V. Cozac, B. Auschra, M. Chaturvedi, U. Gschwandtner, F. Hatz, A. Meyer, A. Welge-Lüssen, P. Fuhr, Among early appearing non-motor signs of parkinson's disease, alteration of olfaction but not electroencephalographic spectrum correlates with motor function, Front. Neurol. 8 (2017) 545, https://doi.org/10.3389/fneur.2017.00545.
[33] J. Lötsch, T. Hummel, The clinical significance of electrophysiological measures of olfactory function, Behav. Brain Res. 170 (2006) 78–83, https://doi.org/10.1016/j.bbr.2006.02.013.
[34] S. Barz, T. Hummel, E. Pauli, M. Majer, C.J.G. Lang, G. Kobal, Chemosensory event-related potentials in response to trigeminal and olfactory stimulation in idiopathic Parkinson's disease, Neurology. 49 (1997) 1424–1431, https://doi.org/10.1212/WNL.49.5.1424.
[35] B. Herting, S. Schulze, H. Reichmann, A. Haehner, T. Hummel, A longitudinal study of olfactory function in patients with idiopathic Parkinson's disease, J. Neurol. 255 (2008) 367–370, https://doi.org/10.1007/s00415-008-0665-5.
[36] A. Welge-Lüssen, E. Wattendorf, U. Schwerdtfeger, P. Fuhr, D. Bilecen, T. Hummel, B. Westermann, Olfactory-induced brain activity in Parkinson's disease relates to the expression of event-related potentials: a functional magnetic resonance imaging study, Neuroscience. 162 (2009) 537–543, https://doi.org/10.1016/j.neuroscience.2009.04.050.
[37] V.A. Schriever, P. Han, S. Weise, F. Hösel, R. Pellegrino, T. Hummel, A. Mouraux, Time frequency analysis of olfactory induced EEG-power change, PLoS One. 12 (10) (2017) e0185596.
[38] M. Ahmadi, R. Quian Quiroga, Automatic denoising of single-trial evoked potentials, Neuroimage. 66 (2013) 672–680, https://doi.org/10.1016/j.neuroimage.2012.10.062.
[39] C.H. Wu, P.L. Lee, C.H. Shu, C.Y. Yang, M.T. Lo, C.Y. Chang, J.C. Hsieh, Empirical mode decomposition-based approach for intertrial analysis of olfactory event-related potential features, Chemosens. Percept. 5 (2012) 280–291, https://doi.org/10.1007/s12078-012-9134-8.
[40] C. Güdücü, B.O. Olcay, L. Schäfer, M. Aziz, V.A. Schriever, M. Özgören, T. Hummel, Separating normosmic and anosmic patients based on entropy evaluation of olfactory event-related potentials, Brain Res. 1708 (2019) 78–83, https://doi.org/10.1016/j.brainres.2018.12.012.
[41] J. Frasnelli, B. Schuster, T. Hummel, Interactions between olfaction and the trigeminal system: What can be learned from olfactory loss, Cereb. Cortex. 17 (2007) 2268–2275, https://doi.org/10.1093/cercor/bhl135.
[42] T. Hummel, S. Barz, J. Lötsch, S. Roscher, B. Kettenmann, G. Kobal, Loss of olfactory function leads to a decrease of trigeminal sensitivity, Chem. Senses. 21 (1996) 75–79, https://doi.org/10.1093/chemse/21.1.75.
[43] P. Rombaux, A. Mouraux, T. Keller, T. Hummel, Trigeminal event-related potentials in patients with olfactory dysfunction, Rhinology. 46 (2008) 170–174.
[44] C. Tremblay, P. Durand Martel, J. Frasnelli, Chemosensory perception is specifically impaired in Parkinson's disease, Park. Relat. Disord. 57 (2018) 68–71, https://doi.org/10.1016/j.parkreldis.2018.08.002.
[45] C. Tremblay, P. Durand Martel, J. Frasnelli, Trigeminal system in Parkinson's disease: A potential avenue to detect Parkinson-specific olfactory dysfunction, Park. Relat. Disord. 44 (2017) 85–90, https://doi.org/10.1016/j.parkreldis.2017.09.010.

[46] C. Pappalettera, F. Miraglia, M. Cotelli, P.M. Rossini, F. Vecchio, Analysis of complexity in the EEG activity of Parkinson's disease patients by means of approximate entropy, GeroScience 44 (3) (2022) 1599–1607.
[47] F. Skidmore, D. Korenkevych, Y. Liu, G. He, E. Bullmore, P.M. Pardalos, Connectivity brain networks based on wavelet correlation analysis in Parkinson fMRI data, Neurosci. Lett. 499 (2011) 47–51, https://doi.org/10.1016/j.neulet.2011.05.030.
[48] M. Conti, R. Bovenzi, E. Garasto, T. Schirinzi, F. Placidi, N.B. Mercuri, R. Cerroni, M. Pierantozzi, A. Stefani, Brain Functional Connectivity in de novo Parkinson's Disease Patients Based on Clinical EEG, Front. Neurol. 13 (2022) 369, https://doi.org/10.3389/fneur.2022.844745.
[49] C. Guducu, S. Taslica, R. Cakmur, M. Ozgoren, A.O. Ikiz, A. Oniz, Assessing olfactory function in Parkinson's disease via entropy analysis of chemosensory event related potentials, Tohoku J. Exp. Med. 237 (2015) 111–116, https://doi.org/10.1620/tjem.237.111.
[50] R. Abiri, S. Borhani, E.W. Sellers, Y. Jiang, X. Zhao, A comprehensive review of EEG-based brain-computer interface paradigms, J. Neural Eng. 16 (2019) 11001, https://doi.org/10.1088/1741-2552/aaf12e.
[51] H. Yuan, B. He, Brain-computer interfaces using sensorimotor rhythms: Current state and future perspectives, IEEE Trans. Biomed. Eng. 61 (2014) 1425–1435, https://doi.org/10.1109/TBME.2014.2312397.
[52] N. Naseer, K.S. Hong, fNIRS-based brain-computer interfaces: A review, Front. Hum. Neurosci. 9 (2015) 3, https://doi.org/10.3389/fnhum.2015.00003.
[53] C.Y. Kee, S.G. Ponnambalam, C.K. Loo, Binary and multi-class motor imagery using Renyi entropy for feature extraction, Neural Comput. Appl. 28 (2017) 2051–2062, https://doi.org/10.1007/s00521-016-2178-y.
[54] C. Vidaurre, N. Krämer, B. Blankertz, A. Schlögl, Time Domain Parameters as a feature for EEG-based Brain-Computer Interfaces, Neural Networks. 22 (2009) 1313–1319, https://doi.org/10.1016/j.neunet.2009.07.020.
[55] K.K. Ang, Z.Y. Chin, C. Wang, C. Guan, H. Zhang, Filter bank common spatial pattern algorithm on BCI competition IV datasets 2a and 2b, Front. Neurosci. 6 (2012) 39, https://doi.org/10.3389/fnins.2012.00039.
[56] B. Orkan Olcay, M. Özgören, B. Karaçalı, On the characterization of cognitive tasks using activity-specific short-lived synchronization between electroencephalography channels, Neural Networks. 143 (2021) 452–474, https://doi.org/10.1016/j.neunet.2021.06.022.
[57] R. Yuvaraj, U. Rajendra Acharya, Y. Hagiwara, A novel Parkinson's Disease Diagnosis Index using higher-order spectra features in EEG signals, Neural Comput. Appl. 30 (2018) 1225–1235, https://doi.org/10.1007/s00521-016-2756-z.
[58] U. Raghavendra, U.R. Acharya, H. Adeli, Artificial Intelligence Techniques for Automated Diagnosis of Neurological Disorders, Eur. Neurol. 82 (2020) 41–64, https://doi.org/10.1159/000504292.
[59] N. Yoneyama, H. Watanabe, K. Kawabata, E. Bagarinao, K. Hara, T. Tsuboi, Y. Tanaka, R. Ohdake, K. Imai, M. Masuda, T. Hattori, M. Ito, N. Atsuta, T. Nakamura, M. Hirayama, S. Maesawa, M. Katsuno, G. Sobue, S. Hayasaka, Severe hyposmia and aberrant functional connectivity in cognitively normal Parkinson's disease, PLoS One. 13 (1) (2018) e0190072.
[60] S.B. Lee, Y.J. Kim, S. Hwang, H. Son, S.K. Lee, K. Il Park, Y.G. Kim, Predicting Parkinson's disease using gradient boosting decision tree models with electroencephalography signals, Park. Relat. Disord. 95 (2022) 77–85, https://doi.org/10.1016/j.parkreldis.2022.01.011.
[61] S.H. Jin, P. Lin, M. Hallett, Linear and nonlinear information flow based on time-delayed mutual information method and its application to corticomuscular interaction, Clin. Neurophysiol. 121 (2010) 392–401, https://doi.org/10.1016/j.clinph.2009.09.033.
[62] Z. Liang, S. Oba, S. Ishii, An unsupervised EEG decoding system for human emotion recognition, Neural Networks. 116 (2019) 257–268, https://doi.org/10.1016/j.neunet.2019.04.003.
[63] X.N. Zhang, Q.H. Meng, M. Zeng, H.R. Hou, Decoding olfactory EEG signals for different odor stimuli identification using wavelet-spatial domain feature, J. Neurosci. Methods. 363 (2021), 109355, https://doi.org/10.1016/j.jneumeth.2021.109355.
[64] B. Kara Gulay, N. Demirel, A. Vahaplar, C. Guducu, A novel feature extraction method using chemosensory EEG for Parkinson's disease classification, Biomed. Signal Process. Control. 79 (2023) 104147.
[65] T. Hummel, G. Kobal, H. Gudziol, A. Mackay-Sim, Normative data for the "Sniffin'' Sticks" including tests of odor identification, odor discrimination, and olfactory thresholds: An upgrade based on a group of more than 3,000 subjects", Eur. Arch. Oto-Rhino-Laryngology. 264 (2007) 237–243, https://doi.org/10.1007/s00405-006-0173-0.
[66] M. Ozgoren, U. Erdogan, O. Bayazit, S. Taslica, A. Oniz, Brain asymmetry measurement using EMISU (embedded interactive stimulation unit) in applied brain biophysics, Comput. Biol. Med. 39 (2009) 879–888, https://doi.org/10.1016/j.compbiomed.2009.07.001.
[67] V. Jurcak, D. Tsuzuki, I. Dan, 10/20, 10/10, and 10/5 systems revisited: Their validity as relative head-surface-based positioning systems, Neuroimage. 34 (2007) 1600–1611, https://doi.org/10.1016/j.neuroimage.2006.09.024.
[68] S. Tsuchimoto, S. Shibusawa, S. Iwama, M. Hayashi, K. Okuyama, N. Mizuguchi, K. Kato, J. Ushiba, Use of common average reference and large-Laplacian spatial-filters enhances EEG signal-to-noise ratios in intrinsic sensorimotor activity, J. Neurosci. Methods. 353 (2021), 109089, https://doi.org/10.1016/j.jneumeth.2021.109089.
[69] D.J. McFarland, L.M. McCane, S.V. David, J.R. Wolpaw, Spatial filter selection for EEG-based communication, Electroencephalogr. Clin. Neurophysiol. 103 (1997) 386–394, https://doi.org/10.1016/S0013-4694(97)00022-2.
[70] K.A. Ludwig, R.M. Miriani, N.B. Langhals, M.D. Joseph, D.J. Anderson, D. R. Kipke, Using a common average reference to improve cortical neuron recordings from microelectrode arrays, J. Neurophysiol. 101 (2009) 1679–1689, https://doi.org/10.1152/jn.90989.2008.
[71] E. Shumbayawonda, D. López-Sanz, R. Bruña, N. Serrano, A. Fernández, F. Maestú, D. Abasolo, Complexity changes in preclinical Alzheimer's disease: An MEG study of subjective cognitive decline and mild cognitive impairment, Clin. Neurophysiol. 131 (2020) 437–445, https://doi.org/10.1016/j.clinph.2019.11.023.
[72] K.K. Ang, Z.Y. Chin, H. Zhang, C. Guan, Filter Bank Common Spatial Pattern (FBCSP) in brain-computer interface, in: Proc. Int. Jt. Conf. Neural Networks, 2008: pp. 2390–2397. https://doi.org/10.1109/IJCNN.2008.4634130.
[73] M.J. Sedghizadeh, H. Aghajan, Z. Vahabi, S.N. Fatemi, A. Afzal, Network synchronization deficits caused by dementia and Alzheimer's disease serve as topographical biomarkers: a pilot study, Brain Struct. Funct. 227 (9) (2022) 2957–2969.
[74] O. Aydemir, Olfactory recognition based on EEG gamma-band activity, Neural Comput. 29 (2017) 1667–1680, https://doi.org/10.1162/NECO_a_00966.
[75] T. Meusel, B. Westermann, P. Fuhr, T. Hummel, A. Welge-Lüssen, The course of olfactory deficits in patients with Parkinson's disease-A study based on psychophysical and electrophysiological measures, Neurosci. Lett. 486 (2010) 166–170, https://doi.org/10.1016/j.neulet.2010.09.044.
[76] L.F. Kozachenko, N.N. Leonenko, Sample Estimate of the Entropy of a Random Vector, accessed April 12, 2022, Probl. Inf. Transm. 23 (1987) 95–101, http://www.mathnet.ru/eng/ppi797.
[77] R. Jenke, A. Peer, M. Buss, Feature extraction and selection for emotion recognition from EEG, IEEE Trans. Affect. Comput. 5 (2014) 327–339, https://doi.org/10.1109/TAFFC.2014.2339834.
[78] H. Ramoser, J. Müller-Gerking, G. Pfurtscheller, Optimal spatial filtering of single trial EEG during imagined hand movement, IEEE Trans. Rehabil. Eng. 8 (2000) 441–446, https://doi.org/10.1109/86.895946.
[79] Z.C. Motteler, G. Strang, Linear Algebra and Its Applications, Belmont, CA: Thomson, Brooks/Cole 85 (1) (1978) 59.
[80] B. Blankertz, R. Tomioka, S. Lemm, M. Kawanabe, K.R. Müller, Optimizing spatial filters for robust EEG single-trial analysis, IEEE Signal Process. Mag. 25 (2008) 41–56, https://doi.org/10.1109/MSP.2008.4408441.
[81] R.A. Fisher, the Use of Multiple Measurements in Taxonomic Problems, Ann. Eugen. 7 (1936) 179–188, https://doi.org/10.1111/j.1469-1809.1936.tb02137.x.
[82] V.N. Vapnik, The Nature of Statistical Learning Theory, Nat. Stat. Learn. Theory. (2000), https://doi.org/10.1007/978-1-4757-3264-1.
[83] J.E. Santos Toural, A. Montoya Pedrón, E.J. Marañón Reyes, Classification among healthy, mild cognitive impairment and Alzheimer's disease subjects based on wavelet entropy and relative beta and theta power, Pattern Anal. Appl. 24 (2021) 413–422, https://doi.org/10.1007/s10044-020-00910-8.
[84] C.X. Han, J. Wang, G.S. Yi, Y.Q. Che, Investigation of EEG abnormalities in the early stage of Parkinson's disease, Cogn. Neurodyn. 7 (2013) 351–359, https://doi.org/10.1007/s11571-013-9247-z.
[85] D. Stoffers, J.L.W. Bosboom, J.B. Deijen, E.C. Wolters, H.W. Berendse, C.J. Stam, Slowing of oscillatory brain activity is a stable characteristic of Parkinson's disease without dementia, Brain. 130 (2007) 1847–1860, https://doi.org/10.1093/brain/awm034.
[86] H. Akaike, Fitting autoregressive models for prediction, Ann. Inst. Stat. Math. 21 (1969) 243–247, https://doi.org/10.1007/BF02532251.
[87] M. Emre Cek, M. Ozgoren, F. Acar Savaci, Continuous time wavelet entropy of auditory evoked potentials, Comput. Biol. Med. 40 (2010) 90–96. https://doi.org/10.1016/j.compbiomed.2009.11.005.
[88] O.A. Rosso, S. Blanco, J. Yordanova, V. Kolev, A. Figliola, M. Schürmann, E. Ba ar, Wavelet entropy: A new tool for analysis of short duration brain electrical signals, J. Neurosci. Methods. 105 (2001) 65–75. https://doi.org/10.1016/S0165-0270(00)00356-3.
[89] J. Jin, C. Liu, I. Daly, Y. Miao, S. Li, X. Wang, A. Cichocki, Bispectrum-Based Channel Selection for Motor Imagery Based Brain-Computer Interfacing, IEEE Trans. Neural Syst. Rehabil. Eng. 28 (2020) 2153–2163, https://doi.org/10.1109/TNSRE.2020.3020975.
[90] T. Hummel, B. Sekinger, S.R. Wolf, E. Pauli, G. Kobal, "Sniffin" sticks'. Olfactory performance assessed by the combined testing of odor identification, odor discrimination and olfactory threshold, Chem. Senses. 22 (1997) 39–52, https://doi.org/10.1093/chemse/22.1.39.
[91] B.O. Olcay, B. Karaçalı, Evaluation of synchronization measures for capturing the lagged synchronization between EEG channels: A cognitive task recognition approach, Comput. Biol. Med. 114 (2019), 103441, https://doi.org/10.1016/j.compbiomed.2019.103441.
[92] J. Li, Y. Wang, L. Zhang, A. Cichocki, T.P. Jung, Decoding EEG in Cognitive Tasks With Time-Frequency and Connectivity Masks, IEEE Trans. Cogn. Dev. Syst. 8 (2016) 298–308, https://doi.org/10.1109/TCDS.2016.2555952.
[93] M. Norizadeh Cherloo, H. Kashefi Amiri, M.R. Daliri, Ensemble Regularized Common Spatio-Spectral Pattern (ensemble RCSSP) model for motor imagery-based EEG signal classification, Comput. Biol. Med. 135 (2021), 104546, https://doi.org/10.1016/j.compbiomed.2021.104546.
[94] S.H. Park, D. Lee, S.G. Lee, Filter Bank Regularized Common Spatial Pattern Ensemble for Small Sample Motor Imagery Classification, IEEE Trans. Neural Syst. Rehabil. Eng. 26 (2018) 498–505, https://doi.org/10.1109/TNSRE.2017.2757519.

[95] E. Başar, M. Özgören, A. Öniz, C. Schmiedt, C. Başar-Eroğlu, Brain oscillations differentiate the picture of one's own grandmother, Int. J. Psychophysiol. 64 (2007) 81–90, https://doi.org/10.1016/j.ijpsycho.2006.07.002.

[96] H.R. Hou, X.N. Zhang, Q.H. Meng, Odor-induced emotion recognition based on average frequency band division of EEG signals, J. Neurosci. Methods. 334 (2020), 108599, https://doi.org/10.1016/j.jneumeth.2020.108599.

[97] K. Shen, A. McFadden, A.R. McIntosh, Signal complexity indicators of health status in clinical EEG, Sci. Rep. 11 (2021), https://doi.org/10.1038/s41598-021-99717-8.

[98] H. Adeli, S. Ghosh-Dastidar, N. Dadmehr, A spatio-temporal wavelet-chaos methodology for EEG-based diagnosis of Alzheimer's disease, Neurosci. Lett. 444 (2008) 190–194, https://doi.org/10.1016/j.neulet.2008.08.008.

[99] G.S. Yi, J. Wang, B. Deng, X. Le Wei, Complexity of resting-state EEG activity in the patients with early-stage Parkinson's disease, Cogn. Neurodyn. 11 (2017) 147–160, https://doi.org/10.1007/s11571-016-9415-z.

[100] Y. Benjamini, Y. Hochberg, Controlling the False Discovery Rate: A Practical and Powerful Approach to Multiple Testing, J. R. Stat. Soc. Ser. B. 57 (1995) 289–300, https://doi.org/10.1111/j.2517-6161.1995.tb02031.x.

[101] J. Morrison, Human nose can detect 1 trillion odours, Nature. (2014) 1–2. https://doi.org/10.1038/nature.2014.14904.

[102] C. Bushdid, M.O. Magnasco, L.B. Vosshall, A. Keller, Humans can discriminate more than 1 trillion olfactory stimuli, Science (80-.) 343 (2014) 1370–1372, https://doi.org/10.1126/science.1249168.

[103] I. Savic, Imaging of brain activation by odorants in humans, Curr. Opin. Neurobiol. 12 (2002) 455–461, https://doi.org/10.1016/S0959-4388(02)00346-X.

[104] S.K. Khare, V. Bajaj, U.R. Acharya, Detection of Parkinson's disease using automated tunable Q wavelet transform technique with EEG signals, Biocybern, Biomed. Eng. 41 (2021) 679–689, https://doi.org/10.1016/j.bbe.2021.04.008.

[105] C. Georgiopoulos, S.T. Witt, S. Haller, N. Dizdar, H. Zachrisson, M. Engström, E. M. Larsson, A study of neural activity and functional connectivity within the olfactory brain network in Parkinson's disease, NeuroImage Clin. 23 (2019), 101946, https://doi.org/10.1016/j.nicl.2019.101946.

[106] L. Chenxi, Y. Chen, Y. Li, J. Wang, T. Liu, Complexity analysis of brain activity in attention-deficit/hyperactivity disorder: A multiscale entropy analysis, Brain Res. Bull. 124 (2016) 12–20, https://doi.org/10.1016/j.brainresbull.2016.03.007.

[107] X.-M. Pei, C.-X. Zheng, W.-X. He, J. Xu, Quantitative measure of complexity of the dynamic event-related EEG data, Neurocomputing. 70 (1-3) (2006) 263–272.

[108] J.B. Rowe, Connectivity analysis is essential to understand neurological disorders, Front. Syst. Neurosci. 4 (2010) 144, https://doi.org/10.3389/fnsys.2010.00144.

[109] M.E.M. Elhassanien, W.S. Bahnasy, Y.A.E. El-Heneedy, A.M. Kishk, M. O. Tomoum, K.M. Ramadan, O.A. Allah Ragab, Olfactory dysfunction in essential tremor versus tremor dominant Parkinson disease, Clin. Neurol. Neurosurg. 200 (2021) 106352.

[110] T. Hummel, M. Smitka, S. Puschmann, J.C. Gerber, B. Schaal, D. Buschhüter, Correlation between olfactory bulb volume and olfactory function in children and adolescents, Exp. Brain Res. 214 (2011) 285–291, https://doi.org/10.1007/s00221-011-2832-7.

[111] C. Huart, P. Rombaux, T. Hummel, A. Mouraux, Clinical usefulness and feasibility of time-frequency analysis of chemosensory event-related potentials, Rhinology. 51 (2013) 210–221, https://doi.org/10.4193/Rhino13.007.

[112] U. Khatri, G.R. Kwon, Classification of Alzheimer's Disease and Mild-Cognitive Impairment Base on High-Order Dynamic Functional Connectivity at Different Frequency Band, Mathematics. 10 (2022) 805, https://doi.org/10.3390/math10050805.

[113] X. Ying, An Overview of Overfitting and its Solutions, J. Phys. Conf. Ser., IOP Publishing (2019) 22022, https://doi.org/10.1088/1742-6596/1168/2/022022.

[114] G. Varoquaux, P.R. Raamana, D.A. Engemann, A. Hoyos-Idrobo, Y. Schwartz, B. Thirion, Assessing and tuning brain decoders: Cross-validation, caveats, and guidelines, Neuroimage. 145 (2017) 166–179, https://doi.org/10.1016/j.neuroimage.2016.10.038.

[115] M. Hosseini, M. Powell, J. Collins, C. Callahan-Flintoft, W. Jones, H. Bowman, B. Wyble, I tried a bunch of things: The dangers of unexpected overfitting in classification of brain data, Neurosci. Biobehav. Rev. 119 (2020) 456–467, https://doi.org/10.1016/j.neubiorev.2020.09.036.

[116] J. Onton, M. Westerfield, J. Townsend, S. Makeig, Imaging human EEG dynamics using independent component analysis, Neurosci. Biobehav. Rev. 30 (2006) 808–822, https://doi.org/10.1016/j.neubiorev.2006.06.007.

[117] A. Hyvärinen, E. Oja, Independent component analysis: Algorithms and applications, Neural Networks. 13 (2000) 411–430, https://doi.org/10.1016/S0893-6080(00)00026-5.

[118] H. Varsehi, S.M.P. Firoozabadi, An EEG channel selection method for motor imagery based brain–computer interface and neurofeedback using Granger causality, Neural Networks. 133 (2021) 193–206, https://doi.org/10.1016/j.neunet.2020.11.002.

[119] J. Hlinka, M. Paluš, M. Vejmelka, D. Mantini, M. Corbetta, Functional connectivity in resting-state fMRI: Is linear correlation sufficient? Neuroimage. 54 (2011) 2218–2225, https://doi.org/10.1016/j.neuroimage.2010.08.042.

[120] A. Montalto, L. Faes, D. Marinazzo, MuTE: A MATLAB toolbox to compare established and novel estimators of the multivariate transfer entropy, PLoS One. 9 (10) (2014) e109462.

[121] A. Kraskov, H. Stögbauer, P. Grassberger, Estimating mutual information, Phys. Rev. E 69 (6) (2004).

[122] A. Wilmer, M. de Lussanet, M. Lappe, S. Hayasaka, Time-Delayed Mutual Information of the Phase as a Measure of Functional Connectivity, PLoS One. 7 (9) (2012) e44633.

[123] J.D. Bonita, L.C.C. Ambolode, B.M. Rosenberg, C.J. Cellucci, T.A.A. Watanabe, P. E. Rapp, A.M. Albano, Time domain measures of inter-channel EEG correlations: A comparison of linear, nonparametric and nonlinear measures, Cogn. Neurodyn. 8 (1) (2014) 1–15.

[124] J.W. Xu, H. Bakardjian, A. Cichocki, J.C. Principe, A new nonlinear similarity measure for multichannel signals, Neural Networks. 21 (2008) 222–231, https://doi.org/10.1016/j.neunet.2007.12.039.

[125] W. Liu, P.P. Pokharel, J.C. Principe, Correntropy: Properties and applications in non-Gaussian signal processing, IEEE Trans. Signal Process. 55 (2007) 5286–5298, https://doi.org/10.1109/TSP.2007.896065.

[126] N. Tanik, H.I. Serin, A. Celikbilek, L.E. Inan, F. Gundogdu, Associations of olfactory bulb and depth of olfactory sulcus with basal ganglia and hippocampus in patients with Parkinson's disease, Neurosci. Lett. 620 (2016) 111–114, https://doi.org/10.1016/j.neulet.2016.03.050.

[127] L.I. Boon, V.J. Geraedts, A. Hillebrand, M.R. Tannemaat, M.F. Contarino, C. J. Stam, H.W. Berendse, A systematic review of MEG-based studies in Parkinson's disease: The motor system and beyond, Hum. Brain Mapp. 40 (2019) 2827–2848, https://doi.org/10.1002/hbm.24562.

[128] V. Parma, M. Bulgheroni, T. Scaravilli, R. Tirindelli, U. Castiello, Implicit olfactory processing attenuates motor disturbances in idiopathic Parkinson's disease, Cortex. 49 (2013) 1241–1251, https://doi.org/10.1016/j.cortex.2012.05.017.

[129] Q. Tian, S.M. Resnick, S.A. Studenski, Olfaction Is Related to Motor Function in Older Adults, Journals Gerontol. - Ser. A Biol. Sci, Med. Sci. 72 (2017) 1067–1071, https://doi.org/10.1093/gerona/glw222.

[130] R.B. Mars, F.-X. Neubert, M.P. Noonan, J. Sallet, I. Toni, M.F.S. Rushworth, On the relationship between the "default mode network" and the "social brain", Front. Hum. Neurosci. 6 (2012) 189.

[131] S. Japee, K. Holiday, M.D. Satyshur, I. Mukai, L.G. Ungerleider, A role of right middle frontal gyrus in reorienting of attention: A case study, Front. Syst. Neurosci. 9 (2015) 23, https://doi.org/10.3389/fnsys.2015.00023.

[132] J.K. Olofsson, N.E. Bowman, K. Khatibi, J.A. Gottfried, A Time-Based Account of the Perception of Odor Objects and Valences, Psychol. Sci. 23 (2012) 1224–1232, https://doi.org/10.1177/0956797612441951.

[133] P.R. Karunanayaka, D.A. Wilson, M.J. Tobia, B.E. Martinez, M.D. Meadowcroft, P. J. Eslinger, Q.X. Yang, Default mode network deactivation during odor–visual association, Hum. Brain Mapp. 38 (2017) 1125–1139, https://doi.org/10.1002/hbm.23440.

[134] A. Solodkin, P. Hlustik, E.E. Chen, S.L. Small, Fine modulation in network activation during motor execution and motor imagery, Cereb. Cortex. 14 (2004) 1246–1255, https://doi.org/10.1093/cercor/bhh086.

[135] S. Pilgramm, B. de Haas, F. Helm, K. Zentgraf, R. Stark, J. Munzert, B. Krüger, Motor imagery of hand actions: Decoding the content of motor imagery from brain activity in frontal and parietal motor areas, Hum. Brain Mapp. 37 (2016) 81–93, https://doi.org/10.1002/hbm.23015.

[136] J. Munzert, B. Lorey, K. Zentgraf, Cognitive motor processes: The role of motor imagery in the study of motor representations, Brain Res. Rev. 60 (2009) 306–326, https://doi.org/10.1016/j.brainresrev.2008.12.024.

[137] S. Tinaz, M.G. Courtney, C.E. Stern, Focal cortical and subcortical atrophy in early Parkinson's disease, Mov. Disord. 26 (2011) 436–441, https://doi.org/10.1002/mds.23453.

[138] Y. Soudry, C. Lemogne, D. Malinvaud, S.M. Consoli, P. Bonfils, Olfactory system and emotion: Common substrates, Eur. Ann. Otorhinolaryngol. Head Neck Dis. 128 (2011) 18–23, https://doi.org/10.1016/j.anorl.2010.09.007.

[139] Y. Masaoka, I.H. Harding, N. Koiwa, M. Yoshida, B.J. Harrison, V. Lorenzetti, M. Ida, M. Izumizaki, C. Pantelis, I. Homma, The neural cascade of olfactory processing: A combined fMRI-EEG study, Respir. Physiol. Neurobiol. 204 (2014) 71–77, https://doi.org/10.1016/j.resp.2014.06.008.

[140] J.P. Royet, J. Plailly, Lateralization of olfactory processes, Chem. Senses. 29 (2004) 731–745, https://doi.org/10.1093/chemse/bjh067.

[141] Q. Yang, G. Zhou, T. Noto, J.W. Templer, S.U. Schuele, J.M. Rosenow, G. Lane, C. Zelano, S. Hanslmayr, Smell-induced gamma oscillations in human olfactory cortex are required for accurate perception of odor identity, PLoS Biol. 20 (1) (2022) e3001509.

[142] L.C. Fonseca, G.M.A.S. Tedrus, P.N. Carvas, E.C.F.A. Machado, Comparison of quantitative EEG between patients with Alzheimer's disease and those with Parkinson's disease dementia, Clin. Neurophysiol. 124 (2013) 1970–1974, https://doi.org/10.1016/j.clinph.2013.05.001.

[143] K.J. Stam, D.L.J. Tavy, B. Jelles, H.A.M. Achtereekte, J.P.J. Slaets, R.W. M. Keunen, Non-linear dynamical analysis of multichannel EEG: Clinical applications in dementia and Parkinson's disease, Brain Topogr. 7 (1994) 141–150, https://doi.org/10.1007/BF01186772.

[144] P. Polverino, M. Ajčević, M. Catalan, G. Mazzon, C. Bertolotti, P. Manganotti, Brain oscillatory patterns in mild cognitive impairment due to Alzheimer's and Parkinson's disease: An exploratory high-density EEG study, Clin. Neurophysiol. 138 (2022) 1–8, https://doi.org/10.1016/j.clinph.2022.01.136.

[145] E. Iannilli, S. Wiens, A. Arshamian, H.S. Seo, A spatiotemporal comparison between olfactory and trigeminal event-related potentials, Neuroimage. 77 (2013) 254–261, https://doi.org/10.1016/j.neuroimage.2012.12.057.

[146] D.E. Vaillancourt, K.M. Newell, The dynamics of resting and postural tremor in Parkinson's disease, Clin. Neurophysiol. 111 (2000) 2046–2056, https://doi.org/10.1016/S1388-2457(00)00467-3.

[147] B. Hellwig, S. Häußler, B. Schelter, M. Lauk, B. Guschlbauer, J. Timmer, C. H. Lücking, Tremor-correlated cortical activity in essential tremor, Lancet. 357 (2001) 519–523, https://doi.org/10.1016/S0140-6736(00)04044-7.

[148] R. Levy, W.D. Hutchison, A.M. Lozano, J.O. Dostrovsky, High-frequency synchronization of neuronal activity in the subthalamic nucleus of Parkinsonian patients with limb tremor, J. Neurosci. 20 (2000) 7766–7775, https://doi.org/10.1523/jneurosci.20-20-07766.2000.
[149] L. Yao, P. Brown, M. Shoaran, Resting Tremor Detection in Parkinson's Disease with Machine Learning and Kalman Filtering, in: 2018 IEEE Biomed. Circuits Syst. Conf. BioCAS 2018 - Proc., IEEE, 2018: pp. 1–4. https://doi.org/10.1109/BIOCAS.2018.8584721.
[150] G.M. Zucco, F. Rovatti, R.J. Stevenson, Olfactory asymmetric dysfunction in early Parkinson patients affected by unilateral disorder, Front. Psychol. 6 (2015) 1020, https://doi.org/10.3389/fpsyg.2015.01020.
[151] M. Nezafati, H. Temmar, S.D. Keilholz, Functional MRI Signal Complexity Analysis Using Sample Entropy, Front. Neurosci. 14 (2020), https://doi.org/10.3389/fnins.2020.00700.
[152] M. Fraschini, M. Demuru, A. Crobe, F. Marrosu, C.J. Stam, A. Hillebrand, The effect of epoch length on estimated EEG functional connectivity and brain network organisation, J. Neural Eng. 13 (3) (2016) 036015.
[153] A.T. Walden, A. Contreras Cristan, The phase-corrected undecimated discrete wavelet packet transform and its application to interpreting the timing of events, Proc. R. Soc. A Math. Phys. Eng. Sci. 454 (1998) 2243–2266, https://doi.org/10.1098/rspa.1998.0257.
[154] I.W. Selesnick, R.G. Baraniuk, N.G. Kingsbury, The dual-tree complex wavelet transform, IEEE Signal Process. Mag. 22 (2005) 123–151, https://doi.org/10.1109/MSP.2005.1550194.
[155] T. Ercoli, C. Masala, G. Cadeddu, M.M. Mascia, G. Orofino, A.F. Gigante, P. Solla, G. Defazio, L. Rocchi, Does Olfactory Dysfunction Correlate with Disease Progression in Parkinson's Disease? A Systematic Review of the Current Literature, Brain Sci. 12 (5) (2022) 513.
[156] S.A. Khoshnevis, R. Sankar, Diagnosis of Parkinson's disease using higher order statistical analysis of alpha and beta rhythms, Biomed. Signal Process. Control. 77 (2022), 103743, https://doi.org/10.1016/j.bspc.2022.103743.
[157] A. Singh, R.C. Cole, A.I. Espinoza, D. Brown, J.F. Cavanagh, N.S. Narayanan, Frontal theta and beta oscillations during lower-limb movement in Parkinson's disease, Clin. Neurophysiol. 131 (2020) 694–702, https://doi.org/10.1016/j.clinph.2019.12.399.
[158] H.W. Berendse, D.S. Roos, P. Raijmakers, R.L. Doty, Motor and non-motor correlates of olfactory dysfunction in Parkinson's disease, J. Neurol. Sci. 310 (2011) 21–24, https://doi.org/10.1016/j.jns.2011.06.020.
[159] B. Orkan Olcay, B. Karaçalı, Time-resolved EEG signal analysis for motor imagery activity recognition, Biomed. Signal Process. Control. 86 (2023), 105179, https://doi.org/10.1016/j.bspc.2023.105179.
[160] A. Maffei, P. Sessa, Time-resolved $_{\text{connectivity}}$ reveals the "how" and "when" of brain networks reconfiguration during face processing, Neuroimage: Reports. 1 (2) (2021) 100022.
[161] S. Waninger, C. Berka, M. Stevanovic Karic, S. Korszen, P.D. Mozley, C. Henchcliffe, Y. Kang, J. Hesterman, T. Mangoubi, A. Verma, Neurophysiological Biomarkers of Parkinson's Disease, J. Parkinsons. Dis. 10 (2020) 471–480, https://doi.org/10.3233/JPD-191844.
[162] A. Haehner, T. Hummel, H. Reichmann, Olfactory dysfunction as a diagnostic marker for Parkinson's disease, Expert Rev. Neurother. 9 (2009) 1773–1779, https://doi.org/10.1586/ern.09.115.
[163] K. Hoyles, J.C. Sharma, Olfactory loss as a supporting feature in the diagnosis of Parkinson's disease: A pragmatic approach, J. Neurol. 260 (2013) 2951–2958, https://doi.org/10.1007/s00415-013-6848-8.
[164] A. Khosla, P. Khandnor, T. Chand, A comparative analysis of signal processing and classification methods for different applications based on EEG signals, Biocybern, Biomed. Eng. 40 (2020) 649–690, https://doi.org/10.1016/j.bbe.2020.02.002.
[165] Y. Xiao, K. Xia, H. Yin, Y.-D. Zhang, Z. Qian, Z. Liu, Y. Liang, X. Li, AFSTGCN: Prediction for multivariate time series using an adaptive fused spatial-temporal graph convolutional network, Digit. Commun. Networks. (2022), https://doi.org/10.1016/j.dcan.2022.06.019.
[166] Y. Xiao, H. Yin, Y. Zhang, H. Qi, Y. Zhang, Z. Liu, A dual-stage attention-based Conv-LSTM network for spatio-temporal correlation and multivariate time series prediction, Int. J. Intell. Syst. 36 (2021) 2036–2057, https://doi.org/10.1002/int.22370.
[167] Q. Cheng, Y. Chen, Y. Xiao, H. Yin, W. Liu, A dual-stage attention-based Bi-LSTM network for multivariate time series prediction, J. Supercomput. 78 (2022) 16214–16235, https://doi.org/10.1007/s11227-022-04506-3.